frontiers | Frontiers in Earth Science

TYPE Original Research
PUBLISHED 26 June 2024
DOI 10.3389/feart.2024.1413084

Check for updates

OPEN ACCESS

EDITED BY
Gang Rao,
Southwest Petroleum University, China

REVIEWED BY
Fangbin Liu,
Lanzhou University, China
Peng Shu,
Anhui Earthquake Administration, China

*CORRESPONDENCE
Na Yin,
yinnaeq@qq.com
Yanlin Yang,
yanlin1232022@126.com

RECEIVED 06 April 2024
ACCEPTED 31 May 2024
PUBLISHED 26 June 2024

CITATION
Yu Z, Yin N, Yang Y, Li L and Ma Y (2024), Late Quaternary right-lateral slip rate along the Tangyuan segment of the Yilan–Yitong Fault Zone on the NE China Plain.
Front. Earth Sci. 12:1413084.
doi: 10.3389/feart.2024.1413084

COPYRIGHT
© 2024 Yu, Yin, Yang, Li and Ma. This is an open-access article distributed under the terms of the Creative Commons Attribution License (CC BY). The use, distribution or reproduction in other forums is permitted, provided the original author(s) and the copyright owner(s) are credited and that the original publication in this journal is cited, in accordance with accepted academic practice. No use, distribution or reproduction is permitted which does not comply with these terms.

Late Quaternary right-lateral slip rate along the Tangyuan segment of the Yilan–Yitong Fault Zone on the NE China Plain

Zhongyuan Yu[1,2,3], Na Yin[2]*, Yanlin Yang[1]*, Luwei Li[1] and Yanli Ma[2]

[1]Institute of Disaster Prevention, Langfang, Hebei, China, [2]Heilongjiang Earthquake Administration, Harbin, China, [3]Beijing Disaster Prevention Technology Co., LTD., Langfang, Hebei, China

The slip rate of strike-slip active faults is crucial for fault rupture behavior analysis and seismic hazard assessment. Although many segments of the Yilan–Yitong Fault Zone (YYFZ) in NE China have been strongly deformed since the late Quaternary, little progress has been made on its slip rate. With the help of high-resolution satellite images, detailed field investigations, seismic reflections, and Quaternary chronological dating, we mainly studied the late Quaternary right-slip rate of the YYFZ. Field investigations revealed an ~15 km long by ~1–2 m high-surface scarp belt extending along the Tangyuan graben interior, with a series of sag ponds and small parallel bulges. Research has revealed that the most recent paleoearthquake (~M 7.0) occurred between 2,800± 600 a BP and 1,700 ± 200 a BP, with evidence of coseismic surface rupture. The T2 terrace abandonment age of the Heijin River is approximately 55.13 ± 1.78 ka (OSL), and the maximum cumulative right-lateral offset may reach 110 ± 5 m. Thus, the maximum right-slip rate of the Tangyuan segment of the YYFZ since the late Quaternary is constrained to 1–2 mm/a according to the upper terrace model. This study suggests that the presence of a new fault in the basin interior merits more attention when assessing the influential surface range and earthquake potential along the YYFZ, and the features of "low tectonic loading rate, activity migration in space, and clustering in time separated by ten thousand years of seismic quiescence" observed along the YYFZ are highly important for earthquake model construction and tectonic deformation studies in stable continental regions (SCRs).

KEYWORDS

late Quaternary, slip rate, Yilan–Yitong Fault Zone, NE China, tectonic deformation

1 Introduction

The late Quaternary slip rate of strike-slip faults is an important parameter both in fault rupture behavior analysis and in seismic hazard assessment, especially for stable continental regions (SCRs), where the tectonic loading rates can be ignored or are much lower than those in interplate regions (Calais, et al., 2016 and references therein). However, studies of the late Quaternary slip rate along the strike-slip active faults in SCRs have always been limited by intensive artificial modification and vegetation coverage, which greatly influence earthquake model construction and tectonic deformation style studies in SCRs (Calais, et al., 2016).

The NE China Plain may be a typical area in regard to SCRs, given its low tectonic loading rates, spatial activity migration, weak imprint geology, and the topography of active tectonics (Min et al., 2015a; Yu et al., 2015b; Z. Yu, 2016; Calais, et al., 2016; Yu et al., 2018; Shu et al., 2020; Chen, 2021). The Yilan–Yitong Fault Zone (YYFZ), the northeastern primary branch of the Tancheng–Lujiang Fault Zone (TLFZ) on the NE China Plain, is the largest continental-scale strike-slip active structure in the collision area between the western Pacific Plate and thee Eurasia Plate, with a spacing of ~30 km and a length of ~3,600 km; this zone extends from the Northern China Block through Bohai Bay, the NE China Plain, and into the Russian area (Figure 1A). During the past ~10 years, the TLFZ has been studied intensively because of its great significance for understanding volcanic eruptions, tectonic deformation, and mineral resource exploitation, as well as disaster prevention and risk mitigation in densely inhabited areas with high earthquake potential along the structure (Tang et al., 2010; Mi et al., 2013; Yang et al., 2014; Zhai et al., 2016). Previous studies on this giant structure have focused mainly on its Cenozoic tectonic deformation, stress field processes, and dynamic mechanisms (Tian and Du, 1987; Liu et al., 1993; Ren et al., 1999; Ren et al., 2002; Li et al., 2002; Tong, 2002; Q. Zhang et al., 2005; Sun et al., 2006; Shen et al., 2006; Yang et al., 2007; et al., 2009).

The intense seismicity that has occurred along the TLFZ during the past ~50 years has pushed the structure into the focus of scientific research. More than 10 catastrophic earthquakes have affected the residents and cities along the TLFZ. For example, as documented in history, more than 50,000 people were killed by an M 8.5 earthquake that occurred in Tancheng city in Shandong Province in 1668, the epicenter of which was located in the central segment of the TLFZ. In addition, the 1970 M 7.4 earthquake in Bohai Bay and the 1975 M 7.3 event in Haicheng city in Liaoning Province were also associated with the activity of the TLFZ. Although these earthquakes had obvious spatial jumping characteristics and no more than two historical strong earthquake events have been recorded in the same location, these data still suggest that the TLFZ is a strong seismogenic zone (M≥7) in the eastern region of China.

However, there are no written records or instrumental events of M≥6 earthquakes along the YYFZ, which is generally viewed as an important branch of the TLFZ in NE China (Figure 1B) (Yin and Nie, 1993; Xu and Zhu, 1994; Li et al., 2013; G. Zhu et al., 2015; Yu et al., 2016). Therefore, previous studies have suggested that the YYFZ is weakly active and has only a moderate earthquake generation capacity. In recent years, this traditional viewpoint has been questioned by new studies on the active tectonics and earthquake potential of the YYFZ, which have greatly increased international scientific interest both in the seismogenic faulting behavior and tectonic deformation models in the NE Asian region (Min et al., 2011; Min et al., 2013; Yu et al., 2015a; Z. Yu et al., 2015b; Z. Yu, 2016; Yu et al., 2016; Zhai et al., 2016; Gu et al., 2017; Yu et al., 2018; Shu et al., 2020; Wang et al., 2021). Although recent research has suggested that, at least for partial segments, the YYFZ has experienced strong segmented tectonic deformation and has experienced multiple paleoseismic events (M≥7) since the late Quaternary, little progress has been made on its late Quaternary strike-slip rate because of intensive artificial modification and strong vegetation coverage.

Thus, are there any other newly activated segments of the YYFZ other than the previously observed sections, such as Tonghe, Shulan, and Shangzhi, since the late Quaternary? How about its late Quaternary strike-slip rate and its implications for rupture behavior analysis and seismic potential assessment of slow-slipping and comparably less-active faults and the seismic fortification criterion regions where the population and infrastructure are often ill-prepared in SCRs? This research attempts to answer these unresolved fundamental questions based on a previous preliminary study and integrated field investigations of the active tectonics, seismic reflections, microtopography, and paleoseismicity of the Tangyuan segment of the YYFZ in the late Quaternary. The results of this study will not only aid in the in-depth study of the present tectonic deformation and active tectonic characteristics and the risk of strong earthquakes in NE China but will also contribute to a deeper understanding of continental deformation and the rheological characteristics of the continental lithosphere under the influence of oblique subduction of the western Pacific Plate. Additionally, the results are of great scientific significance for studying the tectonic formation, fault evolution, and regional deformation mechanics of NE Asia.

2 Geologic setting

The TLFZ formed and experienced the first cycle of sinistral slip faulting because of the collision between the North China Craton and the South China Block during the early Mesozoic (Yin and Nie, 1993; Zhu et al., 2009; Zhao et al., 2016; Gu et al., 2017); finally, it extended into NE China, and the YYFZ was born and developed after that time (G. Zhu et al., 2005; G; Zhu, Wang, Gu, Zhang and Liu, 2016; Sun et al., 2006; Gu et al., 2016; 2017). Zheng, Gao, and Zheng (1988) segmented the TLFZ into four sections according to the differences in the geologic structure, evolution, neotectonic, and modern seismic features (Min et al., 2017). Each segment has distinctive geometric characteristics, quantitative kinematic parameters, and seismic activity characteristics. In contrast to the other three segments, the western Yilan–Yitong Fault Zone (YYFZ) had an earthquake with a maximum modern instrumental magnitude of M 5.8 in 1963 in Luobei County near the China–Russia border area. In contrast, the eastern Dunhua–Mishan Fault Zone (DDFZ) connects a series of Neogene basalt and Quaternary basins without active faults at the surface (Zhang and Wang, 1995; Zhang et al., 2014; Yu et al., 2015a; 2015b; Yu, 2016) (Figure 1). The latest deep seismic reflections across the northern part of the structure, the location of which is marked with a black dashed line in Figure 1B, reveal that the faults formed a large-scale flower structure with a distinctive Moho offset in the middle (Xu et al., 2017; Zheng et al., 2022) (Figure 2).

In the planar view, the NE–SW-trending, nearly 1,100-km-long YYFZ extends from Shenyang, Changchun, and Harbin to Russia after exiting the Bohai Gulf and entering the land (Deng, Ran, Yang, Min and Chu, 2007) (Figure 1B). Two nearly parallel boundary faults of the YYFZ with a spacing of 5–30 km could be delineated as long, narrow grabens along its strike (Geology and Mineral Resources Bureau of Heilongjiang Province, 1993; Huang and Zhao, 2006; Li et al., 2013; Gu et al., 2017) (Figure 1B).

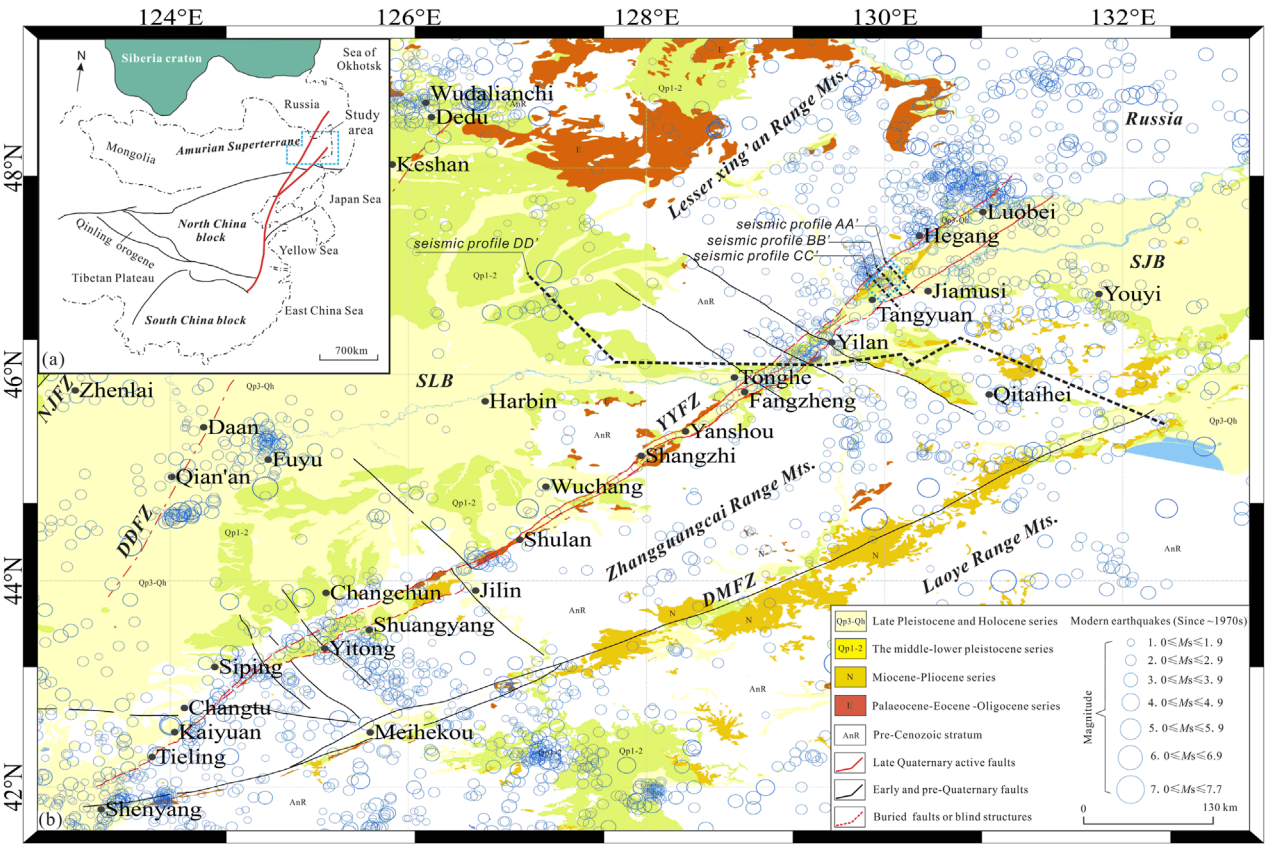

FIGURE 1
Seismotectonic map of NE China and the neighboring area. **(A)** Distribution of the active blocks and the Tancheng–Lujiang Fault Zone (TLFZ, highlighted in red line) in China, modified from Deng et al. (2007) and Yu et al. (2018). **(B)** Seismotectonic map of the YYFZ (Yilan–Yitong Fault Zone) and NE China area. Blue dashed rectangle box in the NE part of the YYFZ indicates the research area of the Tangyuan segment. Blue solid circles represent the distribution of modern earthquakes (Ms≥1.0). Black dashed lines (AA', BB', and CC') near Tangyuan stand for the distribution of artificial seismic detection profiles. Abbreviations: TLFZ (Tancheng–Lujiang Fault Zone); NJFZ (NenJiang Fault Zone); DDFZ (Da'an–Dedu Fault Zone); YYFZ (Yilan–Yitong Fault Zone); DMFZ (Dunhua–Mishan Fault Zone); BBB (Bohai Bay Basin); XLHB (XiaLiaoHe Basin); SLB (SongLiao Basin); SJB (SanJiang Basin).

Generally, the thick Paleogene sediments and Lower Cretaceous sediments are connected by an angular unconformity in the graben (Liu et al., 1993; Tang et al., 2009). Previous studies revealed four secondary grabens from the northeast to southwest, namely, Tangyuan, Fangzheng, Shulan, and Yitong, which are separated by four uplift structures (Gu et al., 2017). The Tangyuan graben is located in the northeastern corner of the YYFZ (Gu et al., 2017) (Figure 1). Wang (2007) reported that the Tangyuan graben includes 5 km of Paleogene sediments, such as the Paleocene Wuyun (E_1w), Eocene Xinancun (E_2x), Eocene Dalianhe (E_2d), and Oligocene Baoquanling (E_3b) formations. The Neogene sediments in the Tangyuan graben are composed of 650 m of the Fujin (N_1-2_f) formation, while the Quaternary sediments are composed of loose sandy conglomerate and mudstone with a thickness of ~50 m (Figure 2).

The architecture of the Tangyuan graben along the YYFZ in the sectional view can be sketched by three parallel seismic profiles, AA', BB', and CC' (Figures 1, 3) (Wang, 2007; Gu et al., 2017), and the locations of the profiles are marked by dashed black lines in Figure 1B. In general, the graben is cut by four major NE-striking faults, named the F1, F2, F3, and F4 faults (Figure 3). The flower structure and a half-graben geometric structure can be observed in the sections, which are bounded mainly by the NE-striking eastern boundary faults. These oil seismic reflection profiles show the stratigraphic deformation characteristics of "east faulting and west superimposition," indicating that the fault deformation of the western boundary was the most intense and played a controlling role in the formation and evolution of the entire graben during the Tertiary period. The profiles also reveal that the DMFZ developed a positive flower structure with a thrust motion, while the YYFZ experienced an inversion from an early negative flower structure to a later positive flower structure because of the change in the regional tectonic stress field in the late Cenozoic (Gu et al., 2017). Although the kinematic features of faults F1, F2, and F3 are strike-slip movements with a normal component in the seismic profiles, the latest rupture of fault F4 is dominated by strike-slip motion with a thrust movement. However, the recent activity characteristics of the Tangyuan graben in the late Quaternary cannot be directly judged by these oil seismic profiles, given their resolution at shallow depths (Figure 3). Thus, the tectonic deformation of these faults in late Quaternary sediments constitutes the focus of this research.

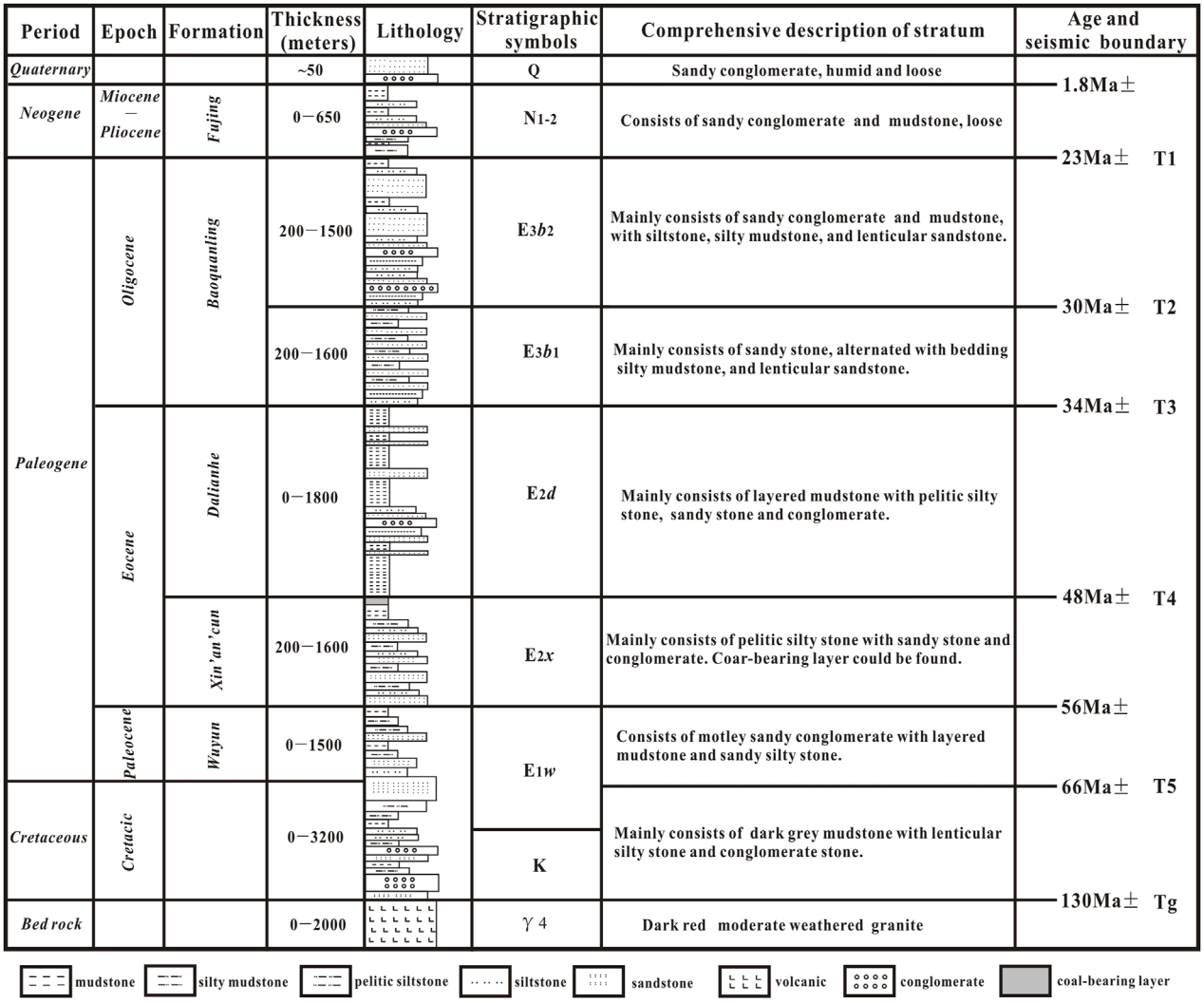

FIGURE 2
General stratigraphic column of the Yilan–Yitong graben (modified from Wang, 2007; Yu et al., 2018).

3 Methods and data

Integrated methods and data are adopted in this research, including interpretations of high-resolution satellite images, surface geological investigations, geomorphic surveys and mapping, trench excavations and logs, dating of OSL and ^{14}C samples, UAV aerial surveys, reinterpretations of high-resolution seismic reflections collected from Daqing Oil Company, and the recollection and reanalysis of previous studies and earthquake catalogs of the YYFZ.

Landsat satellite images are first selected and interpreted in this study (Figure 4). All the sites are composed of distinguishable Late Pleistocene sediments that can yield data about the active deformation of the fault. In contrast to previous studies (Yu et al., 2018), this study selects the river terraces of the Heijin River, a first-level tributary of the Songhuajiang River that flows through the Tangyuan graben in NE China, as the key research object of the study and carries out detailed geomorphological investigations and large-scale trench excavation verification across the structure, which lays an important foundation for the study of the strike-slip rate of the fault since the late Quaternary.

Research on trenches is the first and foremost research method that provides a solid basis for further discussion of the active deformation of the structures. Three trenches are excavated perpendicular to the structural belt after careful position selection based on the preparation of the indoor preview and interpretation of high-resolution satellite images (Figures 5–10). The sizes of the sedimentary particles in the trench logs are classified according to Huggett (2011). Each separate photograph is merged into a mosaic body with grids of photographs in professional software for large-scale geologic mapping (Vanneste et al., 1999; Houtgast et al., 2005; Philip et al., 2012), and all of the stratigraphic characteristics and tectonic deformation are directly recognized in the field again with the integrated mosaic photographs in hand.

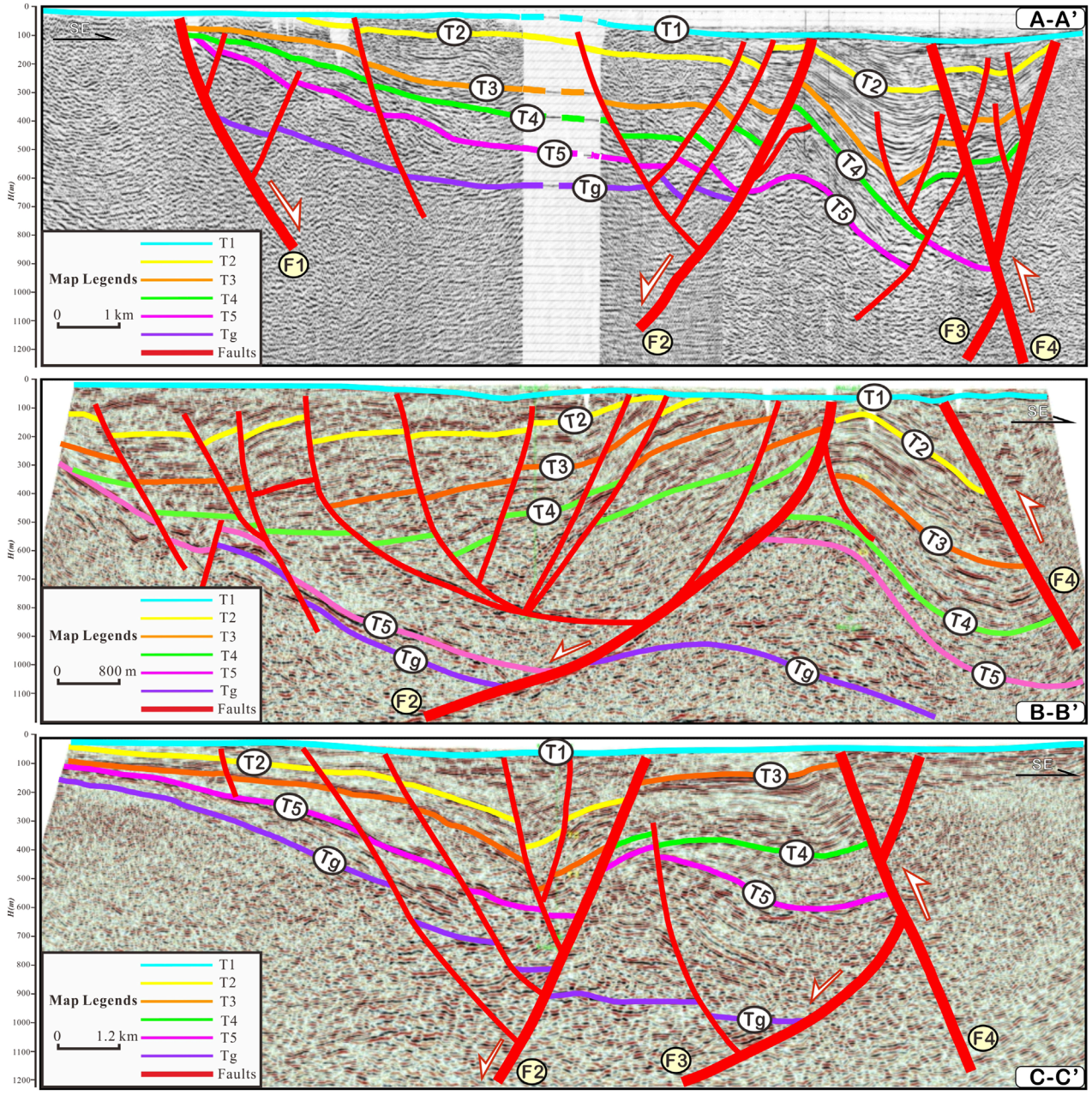

FIGURE 3
Tectonic interpretation profiles of oil seismic prospecting lines. Reflectors T1, T2, T3, T4, T5, and Tg in the profiles stand for the Quaternary sediments, Neogene series, upper Oligocene series, lower Oligocene series, middle-upper Eocene series, Paleocene sediments, and the bed rock, respectively. Faults F1–F4 of the YYFZ (modified from Wang, 2007). The locations of the profile **(AA'–CC')** are marked in dashed black lines in Figure 1B.

Faulting events are discerned based on the disturbed sediments and layers and the microgeomorphic evidence of surface deformation. The horizontal displacement of the river terrace is obtained directly by a high-precision UAV aerial survey, while the vertical displacement is measured according to lined grids and a steel measuring tape in trenches (Audemard et al., 1999; Cetin et al., 2003; Lafuente, et al., 2011). The UAV equipment used in this research is a DJI Phantom 4 RTK, with a flight height of 120 m, a sampling interval of 0.1 s, an effective number of pixels of 20.0 million, a maximum resolution of 4,000×3,000, a 24-mm-wide angle lens, and a camera lens of 94° 20 mm. Data processing and analysis are mainly carried out by professional software applications such as PhotoScan, and geomorphic marker recognition and displacement measurements are carried out on the processed images. The accuracy of the obtained data supports the existing research results.

The shallow artificial seismic reflection method is used in this study, although the collected oil seismic reflection profile reveals its deep structural characteristics. In the field, an ~2 km long survey line is established to the north of Shenli village. The position of the

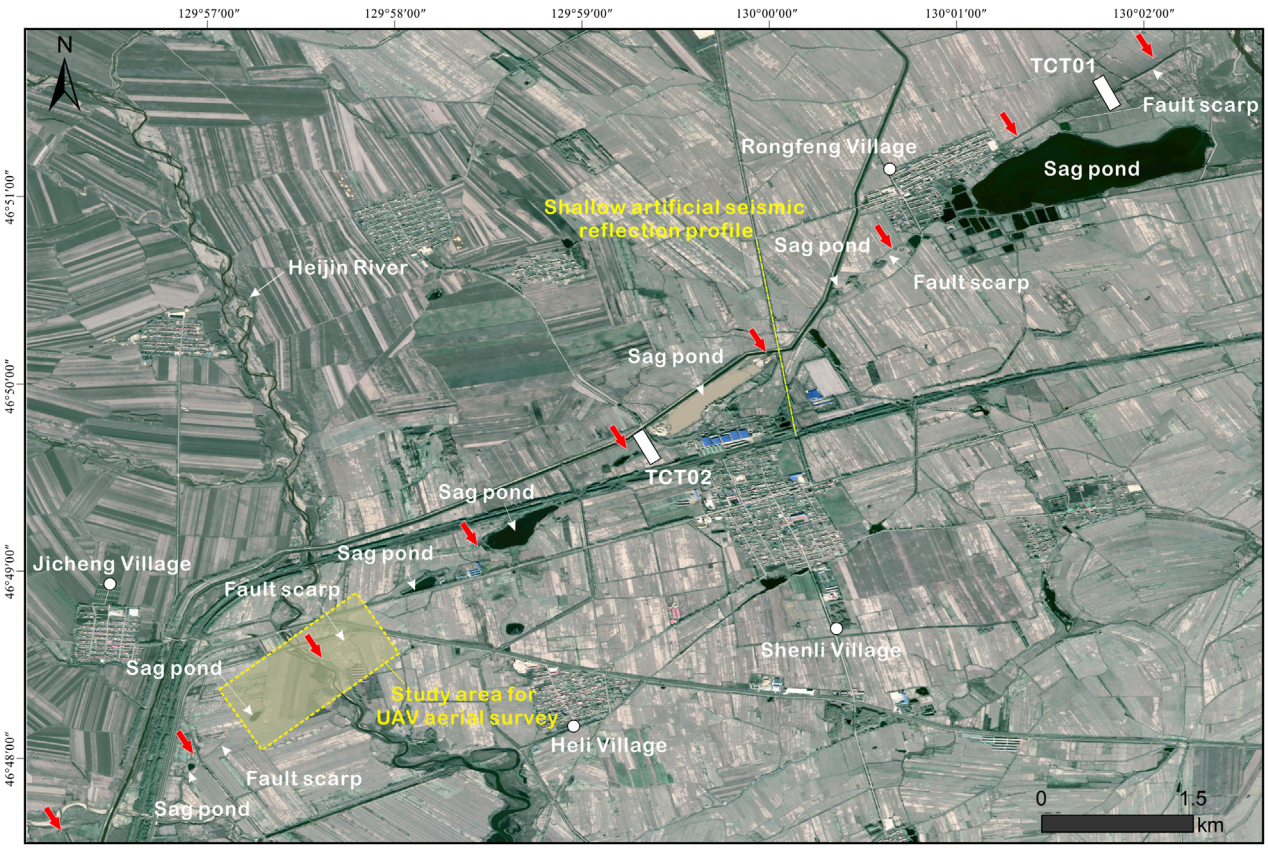

FIGURE 4
Interpreted Spot-5 satellite image of the Tangyuan part along the YYFZ. Red arrows in the map indicate the strike of fault scarps and sag ponds. White hollow rectangles stand for the location of trenches dug across the fault traces, which are interpreted based on the satellite images. The yellow dashed rectangle box in the lower left corner highlights the study area for the UAV aerial survey, while the yellow dashed line spread in the nearly N–S direction to the north of the Shenli village marks the location of the shallow artificial seismic detection profile.

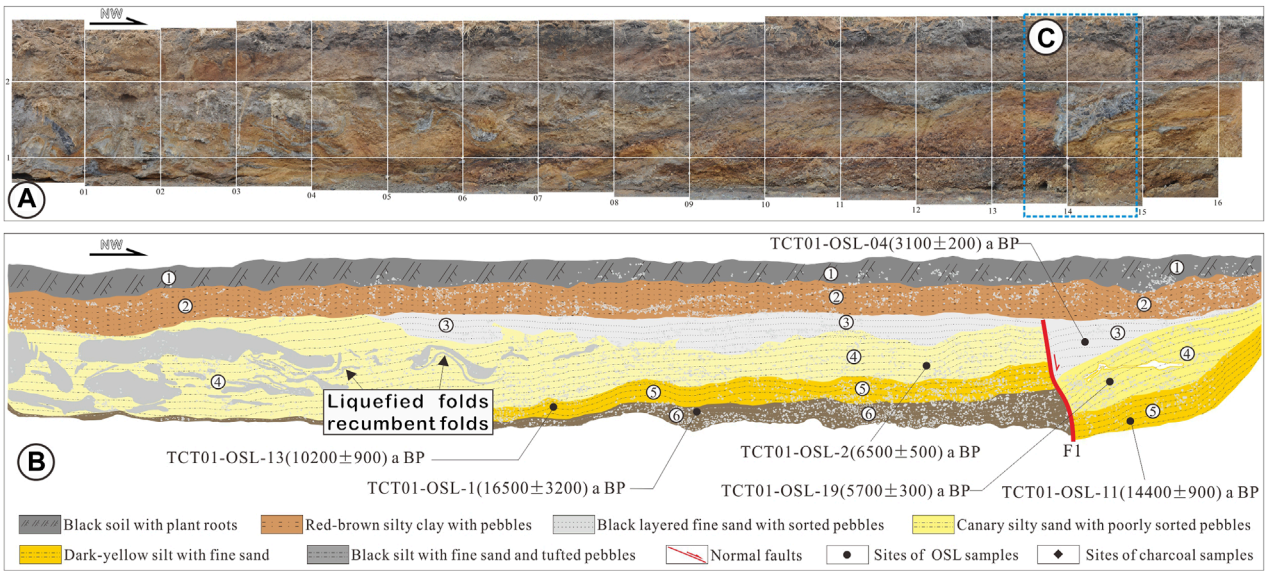

FIGURE 5
Trench logs of TCT01 to the east corner of the Rongfeng village along the NE Tangyuan segment of the YYFZ. **(A)** Profile of the east wall. **(B)** Interpretation map of the east wall. The tectonic activity of the fault resulted in liquefied folds and recumbent folds, as well as the vertical displacement of the corresponding stratum. **(C)** Detailed part are zoomed in on Figure 6.

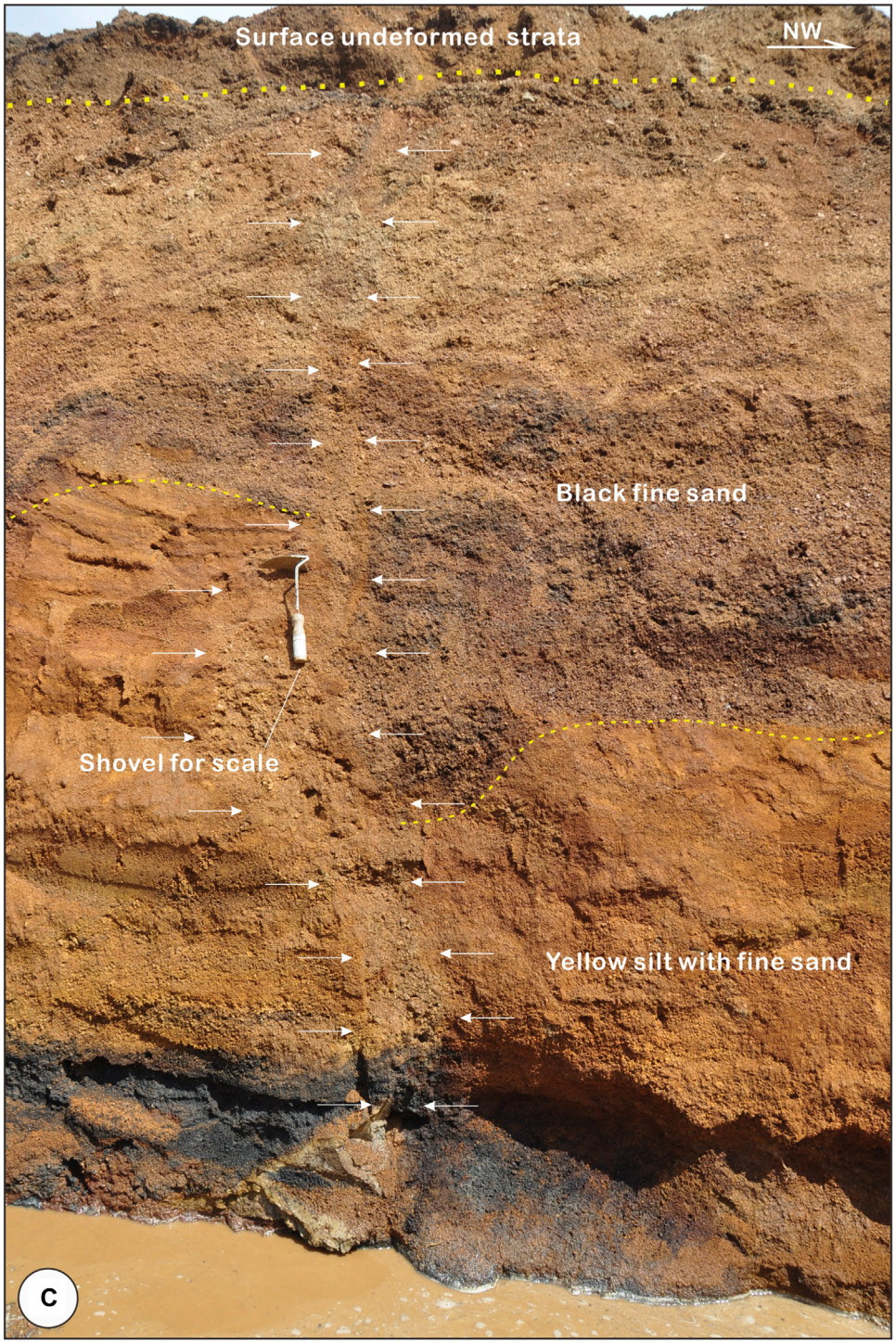

FIGURE 6
Enlarged picture in TCT01 of Figure 5A to the east corner of Rongfeng village. Note the pink pencil in the picture for scale; white arrows in the middle indicate the fault line. The picture reveals the gravels aligned along the main fault plane.

reflection profile is shown in Figure 4. The seismic reflection signal is activated by a 24-ton vehicle source, with 64 channels and 2-m intervals in space in the field. Finally, the filtered and corrected waveforms are used to interpret the recent deformation of the fault in the basin interior (Figure 8).

How to constrain the ages of the latest tectonic deformation is another key point. It is generally accepted that the age of the youngest strata affected and the age of the oldest strata not subjected to deformation could be used to limit the event age. Based on this simple assumption, ^{14}C and optically stimulated luminescence

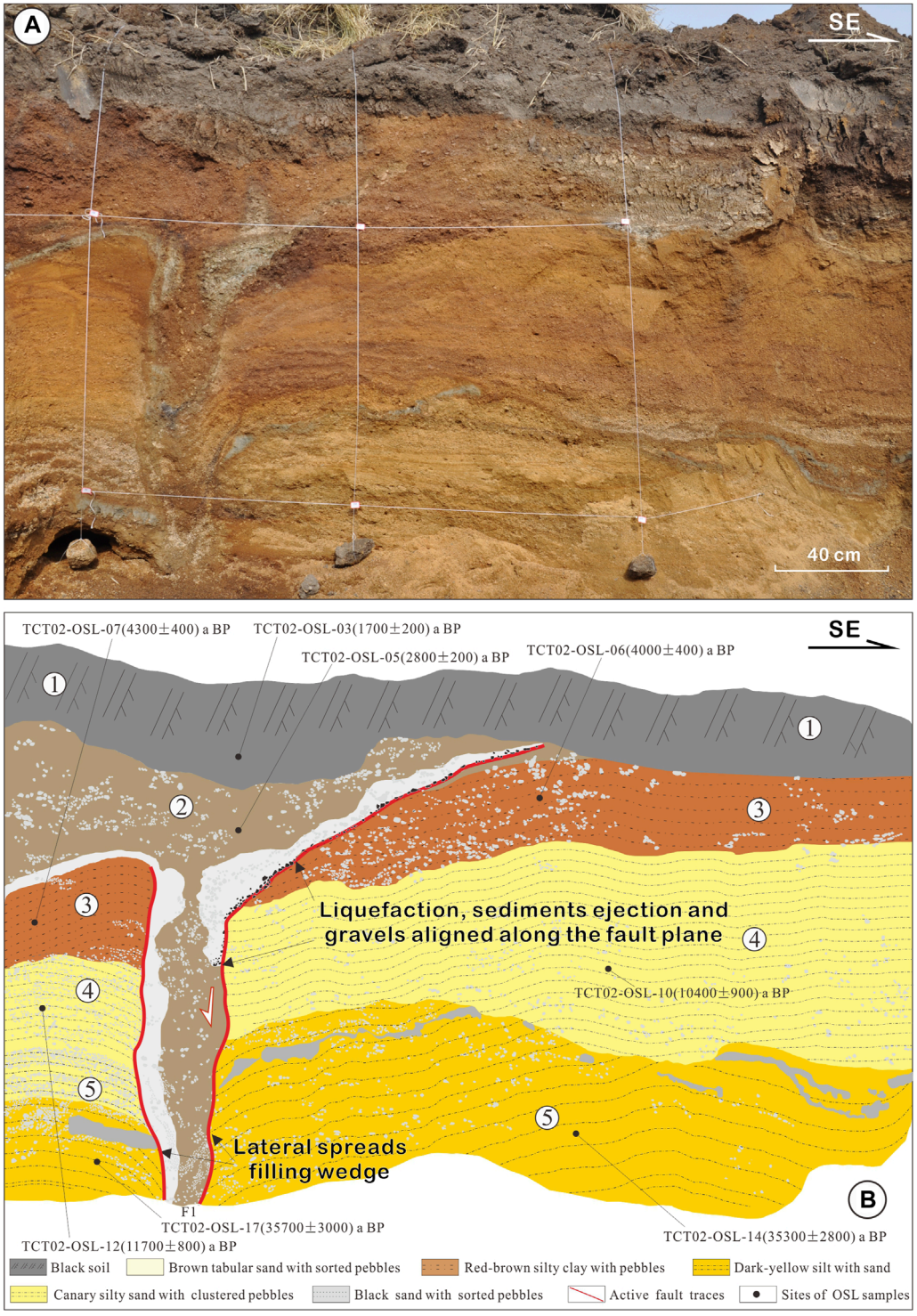

FIGURE 7
Trench logs of TCT02 to the northwest of Rongfeng village, Tangyuan segment of YYFZ. **(A)** Profile of the east wall. **(B)** Interpretation results of the east wall. Interpreted profile reveals that the recent activity of the fault created tension cracks, which were filled with clay and gravels. In addition, the tectonic deformation features such as liquefaction, sediments ejection, and gravels aligned along the fault plane are developed.

(OSL) samples are collected in the field. To prevent the samples from being exposed or contaminated, the ^{14}C samples are sampled and packaged in the field with professional tools and sampling bags. The OSL samples are collected horizontally into the excavated soil through a 30-cm-long stainless-steel tube, and both ends of the tube are sealed with tin foil to ensure no exposure. All of the ^{14}C samples are tested by Beta Analytic, Inc., in the United States. All dating samples for OSL are jointly measured at the Institute of

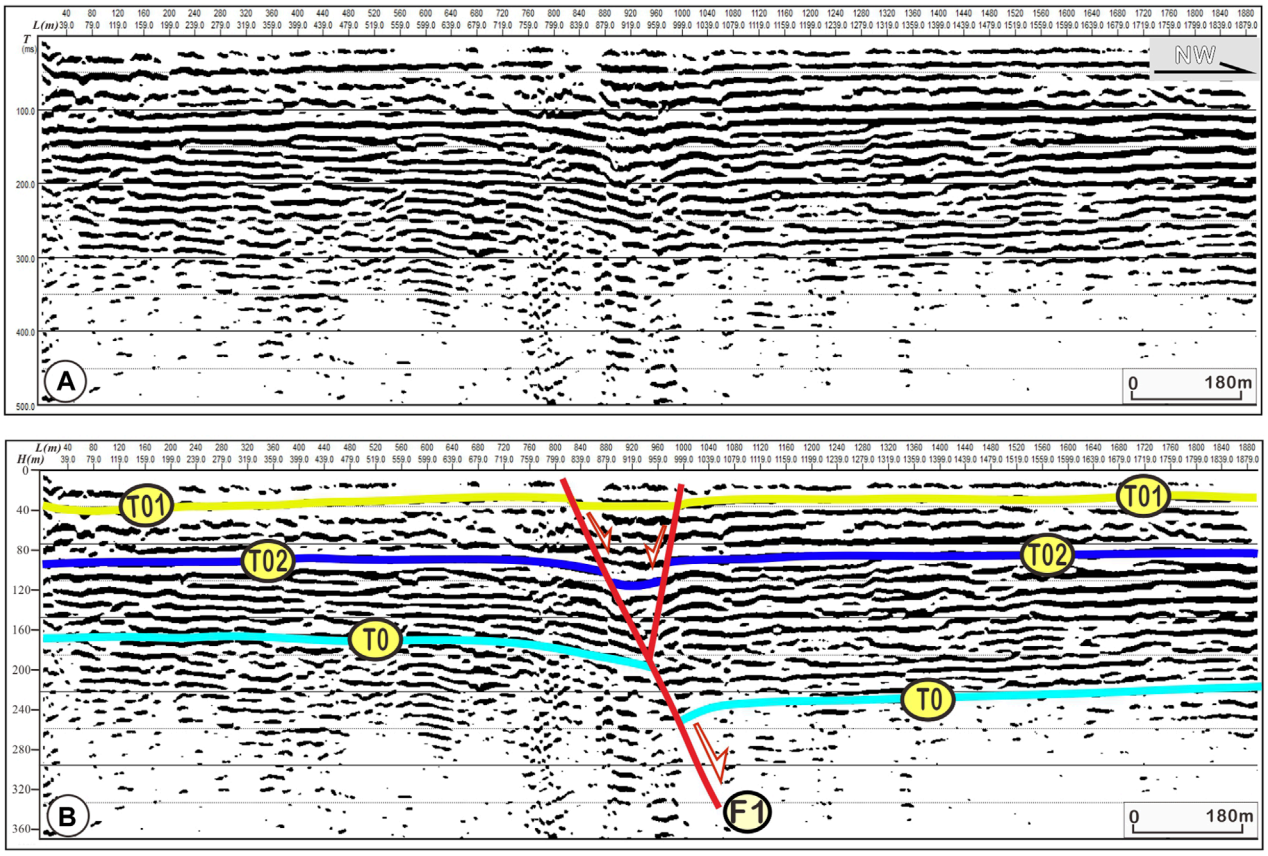

FIGURE 8
Tectonic interpretation profiles of the shallow artificial seismic prospecting line. The location of the profile is marked in a dashed yellow line in Figure 4. **(A)** Below is the interpretive profile. The red lines in the profile represent the interpreted active faults, while the yellow, blue, and green lines in the map represent different reflective interfaces. **(B)** The interpreted profile reveals that the late Quaternary sediments are displaced by the tectonic deformation of the fault F1. The displacement difference of the different reflecting interfaces shows that the tectonic deformation of the fault has been going on since the Quaternary era.

Disaster Prevention and the Institute of Geology, China Earthquake Administration (IGCEA), through the sensitivity-corrected multiple aliquot regenerative-dose (SMAR) protocol that is widely used in the OSL dating laboratory (Lu et al., 2007; Lu, et al., 2007) (Table 1). Additionally, all of the chronology experiments are conducted in strict accordance with laboratory procedures to ensure that no modern materials are mixed and that no samples are contaminated.

4 Results

4.1 Geometric features of the Tangyuan segment of the YYFZ

Topographically, the Tangyuan graben separates the Sanjiang Basin, the Lesser Xing'an Range, and the Zhangguangcai Range from north to south (Figure 1). The Tangyuan graben is controlled by the two boundary faults of the YYFZ. The width of this graben abruptly increases to ~50 km. Modern sparse earthquakes are mainly concentrated along the transitional zone from the Lesser Xing'an Range to the northwestern boundary fault.

According to the indoor interpretation of high-resolution SPOT-5 satellite images, we observed a linear geomorphic abnormal belt that trends ~N45°E and cuts through the graben interior, which is distributed from the south of Jicheng village to Rongfeng village and has a length of ~15 km (Figure 4). Field investigations revealed a series of sag ponds and small bulges elongated parallel to geomorphic scarps (Yu et al., 2018). Our previous surface investigations revealed a series of scarps that were parallelly distributed along a nearly straight line. Based on the field investigation, the speculated fault trace is delineated by red arrows in the Spot-5 satellite image, while the geomorphic scarps and sag ponds are indicated by thin white arrows (Figure 4).

4.2 Features of the latest tectonic deformation revealed by the trenches

To test whether these geomorphic scarps were the result of fault activity, two trenches, TCT01 and TCT02, were excavated across the inferred fault traces for further inspection of this inference and the detection of the latest activity features of the Tangyuan graben of the YYFZ (Figures 5–7).

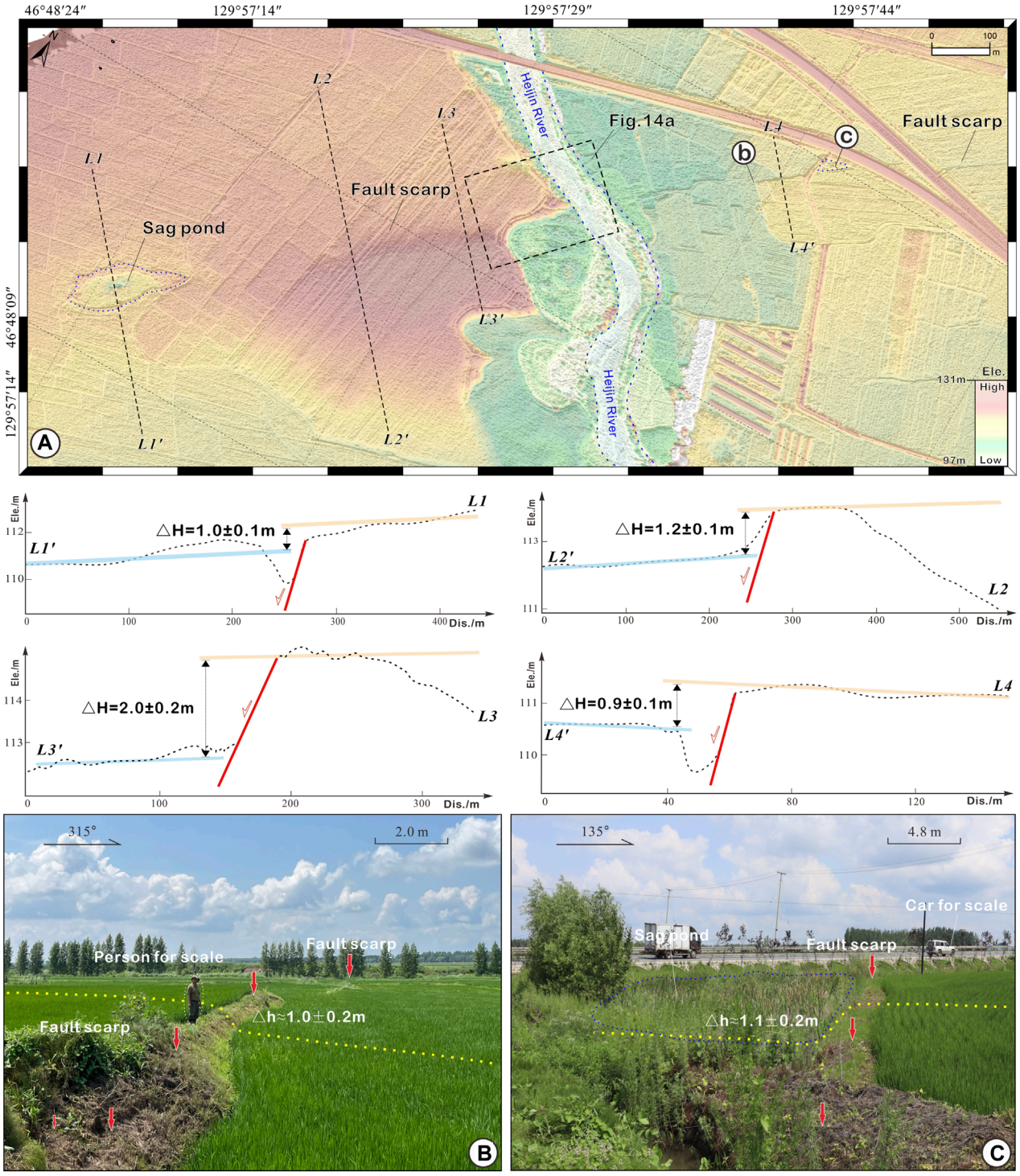

FIGURE 9
General geomorphic features along the SW section of the Tangyuan segment. **(A)** High-resolution digital elevation model (DEM) resulted from UAV survey data. Blue dashed lines delineate the modern course morphology of the Heijin River. Four topographic profiles crossing the river terraces reflect that the new activity of the fault resulted in obvious geomorphic scarps and sag ponds, as shown in the photographs **(B, C)**. Red arrows in the photos highlight the fault scarps. Field survey also shows that the remaining geomorphic scarps are about 1-m-high, although the heights of some individual fault scarps may have been modified by modern farming and industry. Note that the vertical displacement of the T2 terrace surface is approximately 2 m.

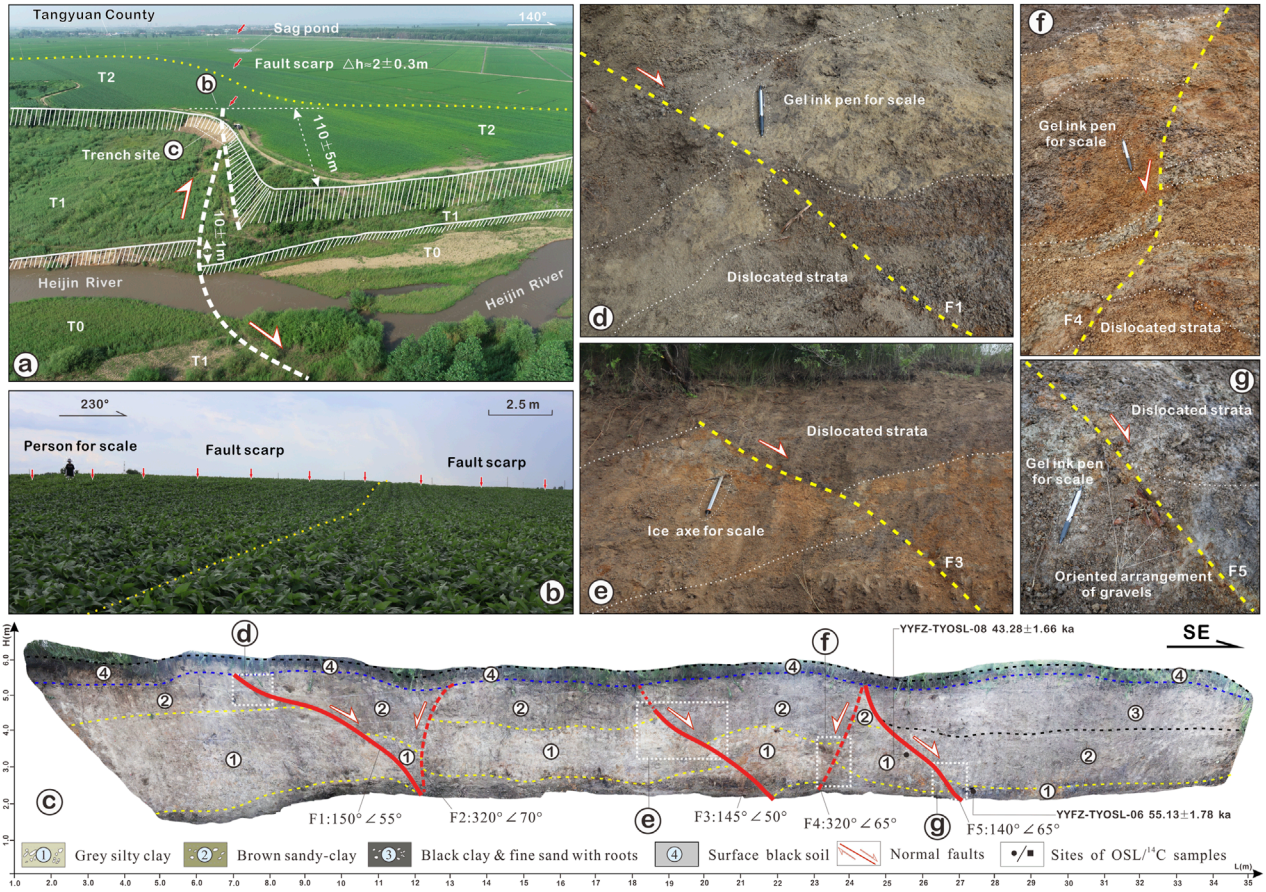

FIGURE 10
Detailed field investigation near the Heijin River (the research scope is delineated by the blue dashed rectangle in Figure 4). **(A)** Aerial photograph obtained by UAV survey shows that the terraces of the Heijin River are displaced by the new activity of the fault. White solid lines in the photograph delineate the terrace risers, while the white dashed lines represent the fault traces. **(B)** Linear fault scarps with the height of ~1.5 m can be observed along the structure. **(C)** Trench log dug across the T2 terrace. **(D–G)** Enlarged photographs show the detailed deformation features observed in the trench profile. Red lines in the profile represent the active faults, while the yellow dashed lines, blue dashed lines, and black dashed lines represent different stratigraphic boundaries.

Trench TCT01 was excavated in the northeastern corner of the inferred fault lines (Figure 4). The TCT01 trench was approximately 17 m long and ~3 m deep (Figure 5), and six types of sediments could be identified based on their components and microstructures, including black soil with plant roots near the surface (unit 1), red-brown silty clay with pebbles (unit 2), black layered fine sand with sorted pebbles (unit 3), canary silty sand with poorly sorted pebbles (unit 4), dark-yellow silt with fine sand (unit 5), and black silt with fine sand and tufted pebbles (unit 6). One of the common characteristics was that unsorted small particles of pebbles and gravels were present in almost all the units.

Only one fault was revealed in trench TCT01, and it is marked as F1 in Figure 5B. Fault F1 was covered by the strata of units 1–2, the thicknesses of which were relatively flat without any evidence of deformation. Thus, it is suggested that the last movement of fault F1 occurred before the sedimentation of units 1–2. Downward, fault F1 cuts units 3–6 normally with a vertical displacement of 0.8 ±0.1 m (Figures 5A–C), which indicates that the latest rupture of fault F1 occurred later than the formation of unit 3. As a result, the latest rupture time of fault F1 can be constrained by the ages of sample TCT01-OSL-04 (3,100 ± 200 a BP).

Trench TCT02 was located in the southwestern part of the inferred fault traces near Helitun village (Figure 7). This trench was approximately 4 m long and ~2.5 m deep (Figures 7A, B), and at least five types of sediments could be identified based on their components and microstructures, including black soil with plant roots near the surface (unit 1), brown tabular sand with sorted pebbles (unit 2), red-brown silt clay with pebbles (unit 3), canary silty sand with clustered pebbles (unit 4), and dark-yellow silt with sand, lenticular black sand, and sorted pebbles (unit 5). Unsorted small particles of pebbles and gravel were clustered in the trench wall (Figure 7).

Fault F1 was directly buried by unit 1 (Figures 7A, B). The strata from unit 3 to unit 5 on both sides of fault F1 matched very well. In contrast to the tectonic deformation revealed by other trenches, the main rupturing features of fault F1 in trench TCT02 included not only a normal offset of 0.3–0.7 m but also

10.3389/feart.2024.1413084

TABLE 1 Measured ages of samples from trenches at the Tangyuan segment along the YYFZ in NE China.

No. in the field	No. in the laboratory	Depth(m)	U-238 (Bg/Kg)	Ra-226 (Bg/Kg)	Th-232 (Bg/Kg)	Water content (%)	Dose rate (Gy/ka)	Eq. dose (Gy)	Age (ka)
TCT01-OSL-01	FZO17-113	1.20	23.4 ± 5.8	10.8 ± 0.5	28.5 ± 0.6	2	5.0 ± 0.5	82.4 ± 5.6	16.5 ± 3.2
TCT01-OSL-02	FZO17-114	0.50	27.5 ± 6.0	13.1 ± 0.5	29.1 ± 0.6	3	4.7 ± 0.5	30.6 ± 2.1	6.5 ± 0.5
TCT01-OSL-04	FZO17-116	0.40	36.0 ± 7.5	14.5 ± 0.6	42.6 ± 0.8	2	5.3 ± 0.5	16.4 ± 1.2	3.1 ± 0.2
TCT01-OSL-11	FZO17-123	1.30	27.5 ± 6.0	17.1 ± 0.5	29.1 ± 0.6	3	4.5 ± 0.5	64.8 ± 4.8	14.4 ± 0.9
TCT01-OSL-13	FZO17-125	0.70	43.6 ± 8.3	33.8 ± 0.7	54.4 ± 1.0	6	4.0 ± 0.3	40.8 ± 0.9	10.2 ± 0.9
TCT01-OSL-19	FZO17-130	1.10	38.1 ± 6.6	33.8 ± 0.4	50.2 ± 1.0	12	3.4 ± 0.3	19.3 ± 1.2	5.7 ± 0.3
TCT02-OSL-14	FZO17-126	2.00	50.4 ± 5.5	37.8 ± 0.6	35.9 ± 0.7	9	3.4 ± 0.3	120.0 ± 8.2	35.3 ± 2.8
TCT02-OSL-12	FZO17-124	1.00	36.0 ± 7.5	14.5 ± 0.6	42.6 ± 0.8	7	3.6 ± 0.3	42.1 ± 2.6	11.7 ± 0.8
TCT02-OSL-03	FZO17-115	0.25	28.1 ± 6.7	25.9 ± 0.6	50.3 ± 0.8	4	3.6 ± 0.2	6.1 ± 0.6	1.7 ± 0.2
TCT02-OSL-17	FZO17-129	2.25	40.1 ± 6.7	26.9 ± 0.6	48.6 ± 1.0	6	3.8 ± 0.3	136.1 ± 9.2	35.7 ± 3.0
TCT02-OSL-05	FZO17-117	0.40	51.1 ± 9.9	19.9 ± 0.8	50.4 ± 1.0	12	4.6 ± 0.5	12.9 ± 1.0	2.8 ± 0.2
TCT02-OSL-06	FZO17-118	0.42	43.6 ± 8.3	23.8 ± 0.7	54.4 ± 1.0	7	4.7 ± 0.5	18.7 ± 1.5	4.0 ± 0.4
TCT02-OSL-07	FZO17-119	0.45	41.1 ± 6.7	23.9 ± 0.6	52.3 ± 0.8	14	3.8 ± 0.3	16.4 ± 1.3	4.3 ± 0.4
YYFZ-TYOSL-01	FZ23-91	1.06	2.33 ± 0.13	12.36 ± 0.09	2.13 ± 0.05	13	3.91 ± 0.3	64.06 ± 0.9	16.38 ± 0.49
YYFZ-TYOSL-06	FZ23-92	3.00	1.48 ± 0.15	12.46 ± 0.09	2.44 ± 0.03	13	3.90 ± 0.3	215.09 ± 2.9	55.13 ± 1.78
YYFZ-TYOSL-07	FZ23-93	1.00	1.65 ± 0.15	13.49 ± 0.09	1.98 ± 0.04	16	3.67 ± 0.2	84.52 ± 5.1	23.04 ± 0.70
YYFZ-TYOSL-08	FZ23-94	4.50	1.85 ± 0.10	14.01 ± 0.09	2.16 ± 0.04	12	3.88 ± 0.3	167.72 ± 8.2	43.28 ± 1.66

All optically stimulated luminescence (OSL) samples are tested by the Institute of Geology in the China Earthquake Administration (IGCEA) and the Institute of Disaster Prevention of China Earthquake Administration. The sensitivity-corrected multiple aliquot regenerative-dose (SMAR) method is adopted in this measurement process (Lu et al., 2007). All measurements were performed using a Daybreak 2200 automated OSL reader equipped with a combined blue (470 ± 5 nm) and infrared (880 ± 80 nm) LED OSL unit, two 90Sr/90Y beta sources (0.19 and 0.157 Gy/s), and an Am-241 alpha source (0.062 μm−2 s−1) for irradiations.

other features of coseismic deformation, such as liquefaction, water ejection, vented sediment, lateral spreads, and some types of soft-sediment deformation (Figures 7A, B). The relationship between this coseismic deformation and the latest activity of the YYFZ is further analyzed in the Discussion section. Nine effective dating samples were collected from this trench, which constrains the age of the latest movement of fault F1. The latest movement of fault F1 should not have occurred before the formation of unit 2 and after the deposition of unit 1. In other words, the occurrence time of the last paleoearthquake revealed in trenches can be further limited between

the ages of sample TCT02-OSL-03 (1,700 ± 200 a BP) and sample TCT02-OSL-05 (2,800± 200 a BP).

4.3 Kinematics of the latest movement of the YYFZ in the Tangyuan graben

Although it is widely accepted that the TLFZ experienced many stages of tectonic deformation and that two stages of extensional deformation on the Cenozoic East Asian continental margin might have resulted in widespread extensional deformation (Ren et al., 2002; Yin, 2010), right-slip faulting with a dip slip moment of the latest deformation along the structure was recently observed in NE China (Min et al., 2013; Yu, 2016; Yu et al., 2016; Zhai et al., 2016; Gu et al., 2017). There are many other pieces of evidence, such as focal mechanisms of strong earthquakes (M≥7), GPS (global position system) observations, and *in situ* stress measurements, which also support this viewpoint. In addition, several scientists have suggested that dextral strike-slip motion with thrust extrusion has been the main feature in NE China since the late Quaternary because of the nearly east–west compression effect (P. Z. Zhang et al., 2003; Hsiao, Graham and Tilander, 2004; Zhu et al., 2015).

The newly obtained tectonic interpretation profiles of the shallow artificial seismic prospecting line in the Tangyuan graben further support this observation. The location of the profile is marked by a dashed yellow line in Figure 4. As shown in Figure 8, the late Quaternary sediments are vertically displaced by the tectonic deformation of fault F1 in the basin interior. This deformation feature is consistent with the geomorphic features such as the sag pond and fault scarp observed on the surface and with the displacement characteristics observed in the trenches.

The differences in the displacements of the different reflecting interfaces show that the tectonic deformation of the fault has continued since the Quaternary. Additionally, the T01 reflector, which represents an important boundary between the Upper Pleistocene sediments and Middle Pleistocene sediments, was directly displaced normally (Figure 4). Thus, based on the above observations and dating results, the YYFZ in the Tangyuan graben has been active since the Late Holocene. The latest rupture event in the graben interior occurred between 1,700 ± 200 a BP and 2,800± 600 a BP, the kinematics of which are dominated by a right strike-slip movement with a normal component.

4.4 Late Quaternary strike-slip rate of the YYFZ in the Tangyuan graben

The offset river terraces in the Heijin River provide geological constraints for the estimation of the strike-slip rate of the YYFZ (Figures 9–11), although previous research has also carried out preliminary constraints based on the results of trench excavation and the deflection of small streams and GPS surveys (Yu et al., 2016; Shu et al., 2020). With the help of a high-resolution digital elevation model (DEM) derived from UAV survey data, a distinct linear geomorphic scarp with a trend of ~N50°E across the Heijin River, a main tributary of the Tangyuan section of the Songhuajiang River, can be observed (Figure 9A).

In particular, it seems that multiple river terraces were systematically deformed by the tectonic deformation of the structure (Figure 9A). Four topographic profiles crossing the river terraces indicate that the new activity of the fault resulted in obvious geomorphic scarps, and the remaining geomorphic scarps are approximately 1 m high, although the heights of some individual fault scarps may have been modified by modern farming and industry. Note that the vertical displacement of the T2 terrace surface was approximately 2 m. Field investigation further revealed that the rice fields on either side of the scarp have a noticeable difference in elevation. Different sections of scarps are connected by steps, the widths of which vary from ~2 to 5 m (Figures 9B, C). Although modern human farming might have had a significant impact on the preservation and evolution of these geomorphic scarps, it is speculated that these geomorphic scarps were mainly caused by recent fault activity.

To verify this speculation, one trench was excavated at the T2 terrace of the Heijin River, as shown in Figures 9 and 10. The trench log was also used to estimate the slip rate of the structure in the late Quaternary. Two faults formed a fault zone in the form of a step (Figure 10A) passing through the Heijin River and its terraces, and there was a geomorphic scarp and sag pond at a distance. Combining the UAV survey results with the field investigation, the maximum cumulative right-lateral offsets of the T2 terrace and T1 terrace may reach 110 ± 5 m and ~10 ± 1 m, respectively.

The trench was approximately 33 m long and ~4 m deep (Figure 10C), and four types of sediments could be identified based on their differences in components and microstructures: gray silty clay with sorted pebbles (unit 1), brown sand clay with fine sand (unit 2), black clay and fine sand with roots (unit 3), and black soil with plant roots near the surface (unit 4) (Figures 10C–G). In addition to the obvious fault rupture, evidence of coseismic deformation, such as gravel orientation and sand liquefaction near the fault trace, could also be observed (Figures 10D–G).

Five faults were identified according to the cross-cutting relationships and section characteristics of the strata in the profile. Faults F1, F3, and F5 constitute the major structures because they have consistent trends and larger vertical displacements, while faults F2 and F4 could be seen as secondary faults with opposite trends and small offsets. Unit 4, approximately 1.2 m thick near the surface, is the main unit affected by agricultural cultivation today, and its approximate horizontal distribution shows that it has not suffered deformation. A detailed field investigation also revealed that the upper breakpoints of all the faults were covered by unit 1. Faults F1 and F2 are located at the western end of the profile and form a Y-shaped graben. Strata units 2 and 3 were vertically dislocated by approximately 1.2 m. The geometric structure and motion characteristics of faults F3 and F4 in the middle section are very similar to those of F1 and F2. Fault F5, located at the eastern end of the profile, is different from the other faults, given its deformation characteristics. Unit 3 is the youngest of the faulted formations and is rich in plant roots and clay. Additionally, the thickness of unit 3 approximately represents ~0.8 m of the vertical displacement of the fault, although unit 3 in the upper wall was not retained because of denudation and erosion. The vertical displacement of ~0.8 m in formation 3 was inconsistent with that of 1.5 m in formation 1 and formation 2, which suggests that the fault may have experienced at least two stages of active deformation at this location (Figure 10C).

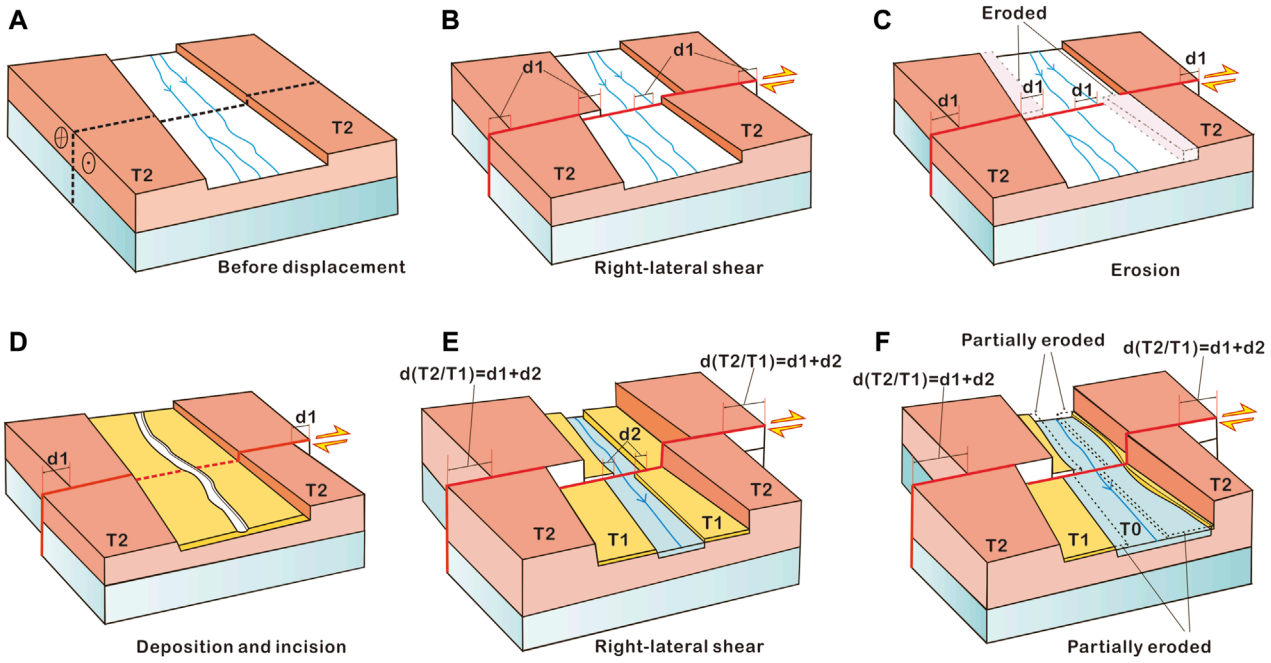

FIGURE 11
Right-lateral strike-slip offset and evolution terraces of the Heijin River flowing toward the readers (modified from Cowgill et al., 2007; Zhang et al., 2007; Li et al., 2008). **(A)** The stream cuts down and erodes laterally to form early river terrace T2. **(B)** River terrace T2 is horizontally displaced by the right-lateral shear of the active fault, resulting in the horizontal displacement d1. **(C)** Lateral erosion of the river has partially or completely eroded the inner terrace T2 on either side of the channel so that the displacement d1 near the river bed cannot be fully preserved. **(D)** River continues to undergo a new round of accumulation and incision process, preparing for the formation of new terrace T1. **(E)** A new right-lateral strike-slip movement occurred on the fault, resulting in the horizontal displacement d2 on the T1 terrace, while the displacement d2+d1 is documented on the outer terrace T2 away from the channel. This process of movement and evolution indicates that the slip rate constrained by the abandonment age of the terrace T2 and the cumulative displacement d2+d1 may be more reasonable. **(F)** Partial erosion may result in incomplete preservation of terrace T1, and river accumulation and the down cutting process is expected to continue in the near future.

The starting time of fault displacement is crucial in the estimation of the corresponding slip rate because of the displacement and upper and lower ages of the corresponding terrace (Cowgill, 2007; Gold et al., 2009; Zhang et al., 2007; 2008; Liu et al., 2021). Generally, the lower terrace model usually provides the upper limit of the slip rate, while the upper terrace model provides the lower limit, given the different erosion degrees of river flow on the terrace scarps in different areas (Zhang et al., 2007; Liu et al., 2021). Therefore, the appropriate terrace reconstruction and evolutionary model first needs to be selected according to the actual situation. A previous study showed that the ages of the upper terraces should more closely approximate the ages of risers than those of the lower terraces in weak erosion cases (Liu et al., 2021).

In NE China, the terrain relief is subtle, and the climate conditions are relatively wet, dry, and cold. Thus, we first reconstructed a model of the right-lateral strike-slip offset and evolutionary terraces of the Heijin River (modified from Cowgill et al., 2007; Zhang et al., 2007; Li et al., 2008; Zhang et al., 2007; 2008; Liu et al., 2021) (Figure 11). According to the terrace model, the stream cut down and eroded laterally to form the early river terrace T2 (Figure 11A). Then, the T2 river terrace was horizontally displaced by the right-lateral shear of the active fault, resulting in the horizontal displacement d1 (Figure 11B). Lateral erosion of the river partially or completely eroded the inner terrace T2 on either side of the channel; therefore, the displacement d1 near the riverbed could not be fully preserved (Figure 11C). Furthermore, the river continued to undergo a new round of accumulation and incision processes, preparing for the formation of the new terrace, T1 (Figure 11D). Then, a new right-lateral strike-slip movement occurred on the fault, resulting in the horizontal displacement d2 on the T1 terrace, while the displacement d2+d1 was documented on the outer terrace T2 away from the channel (Figure 11E). Partial erosion may have resulted in incomplete preservation of terrace T1, and river accumulation and downcutting will continue in the near future (Figure 11F). Under tectonic movement and terrace evolution, it is reasonable that the strike-slip rate of the active fault should be constrained by the abandonment age of terrace T2 and the cumulative displacement d2+d1 (Figure 11).

Two OSL dating samples were collected from this profile to determine the deposition time of the strata and the deformation time of the event (Figure 10C; Table 1). The dating results revealed two important insights. First, the latest deformation of F5 in the T2 terrace likely occurred later than the abandonment of unit 3, although no datable samples could be collected in the field to constrain the deformation time of the event. In addition, the time of the penultimate event could be constrained by the age of formation 1 (YYFZ-TYOSL-06, 55.13 ± 1.78 ka BP and YYFZ-TYOSL-08, 43.28 ± 1.66 ka BP). Thus, the late Quaternary right-slip rate of the structure can be constrained at ~1–2 mm/a if the ~110 ± 5 m maximum cumulative right-lateral offsets of T2 and the age of

formation 1 (YYFZ-TYOSL-06, 55.13 ± 1.78 ka BP and YYFZ-TYOSL-08, 43.28 ± 1.66 ka BP) are considered according to the upper terrace model (Li et al., 2008; Zhang et al., 2008).

5 Discussion

5.1 Recognition of paleoearthquakes on the Tangyuan segment of the YYFZ

Paleoseismic evidence can be classified as primary evidence or secondary evidence according to historical earthquakes (McCalpin, 1996; 2009). The former directly results from coseismic faulting along a specific fault plane (including the growth of fault-related folds) and is equivalent to "seismotectonic deformation," while the latter results from earthquake shaking or from erosional and depositional responses to coseismic elevation changes.

Based on the investigation results, we found that the faulting features discovered along the Tangyuan segment of the YYFZ consisted of linear scarps and troughs, linear sag ponds, small horsts and grabens, a fresh fault plane and fault belt with filling, filling wedge and fissure filling (Figures 5, 6), faulted strata (Figures 5–8), and folded strata (Figure 5), which indicates that this morphologic and sedimentologic evidence of ground deformation should be viewed as primary paleoseismic evidence of the latest activity along the Tangyuan segment of the YYFZ in the late Quaternary. In addition, secondary evidence could also be observed in our research. Liquefaction was most obvious in trench TCT02 (Figure 7). The strong ground shaking that occurred during this paleoearthquake in the Tangyuan graben of the YYFZ caused obvious liquefaction and sediment ejection (Figure 7), which likely resulted from the increased pore pressure that originated from the earthquake shaking, and the strength and stiffness of the unconsolidated sediments may have weakened along the seismic faults and their surrounding regions during the seismic process.

Trench TCT02 was excavated along the major fluvial terraces of the Songhuajiang River, where the water table is only ~3 m below the surface. During coseismic liquefaction, the state of the terrace deposit changes from solid-like to viscous, liquid-like material. Therefore, as shown in Figure 7, the gray-black deposits vented to the ground surface through unit 2 but covered by unit 1 provide the most conspicuous evidence of liquefaction at depth. In addition, a water–sand–small gravel–silt mixture erupted and flowed violently to the surface through fractures opened in the capping material in the liquefaction caused by fault F1 and then covered by unit 1. At the same time, the sediment remaining in the vents through the cap formed a linear clastic dike, which is marked in Figure 7. These gravels are aligned along the main fault plane. Thus, we suggest that nearly active fault earthquakes augmented the coseismic liquefaction intensity in the graben and that the underlying mechanism could be shaking amplification resulting from a specific fault zone. In other words, an unenclosed fault plane may provide a pathway with increased vertical permeability for fluids to migrate from deeper confined aquifers to the upper soil and then induce liquefaction during an earthquake (Figure 7) (Liu et al., 2017).

Other secondary evidence, such as lateral spreading and soft-sediment deformation, could also be observed in our research. Lateral spreading with a width of ~30 cm in the upper layer but narrowing to ~10 cm downward into liquefied sand strata was revealed in trench TCT02 (Figure 7). Soft-sediment deformation such as liquefied folds and recumbent folds also formed on the left side of the trenches. Although the precise date of formation of this soft-sediment deformation could not be constrained directly in our research, they should have originated from paleoearthquakes that occurred along the YYFZ in the Tangyuan graben in the late Quaternary.

In summary, all this primary and secondary morphological or sedimentologic evidence suggests that the Tangyuan segment of the YYFZ underwent strong tectonic deformation in the late Quaternary.

5.2 Estimated magnitude of paleoearthquakes on the Tangyuan segment of the YYFZ

In our research, two empirical methods were adopted for the estimation of the size of the latest fault along the Tangyuan graben of the YYFZ in the Late Holocene. One was based on the empirical statistical relation between the magnitude of a historical earthquake and the surface rupture length, and the other was calculated primarily based on a semiquantitative comparison of the earthquake intensity with the results of historical earthquakes of known magnitudes.

Although much evidence is used to estimate the magnitudes of paleoearthquakes, the coseismic surface rupture length and the maximum displacement on fault traces are by far the most commonly accepted parameters (Wells and Coppersmith, 1994; McCalpin, 1996; Yeats, Sieh and Allen, 1997). Observations and measurements of coseismic rupture length and slip distance during historical earthquakes with known magnitudes have further proved that this method is reliable and acceptable (Deng, Yu and Ye, 1992; McCalpin, 1996, 2009; P. Z. Zhang, 2013; Wesnousky et al., 2006). Many scientists have studied the empirical relationships between the magnitude of an earthquake (M), the length of the surface rupture (L), and displacement (D) (Tocher, 1958; Deng et al., 1992; Wells and Coppersmith, 1994; McCalpin, 1996; 2009; Yeats et al., 1997). In this study, this fitted function is adopted and defined as follows:

$M = 5.90 + \lg L + \lg D$ (Eq. 1; Deng et al., 1992).

M represents the magnitude of the earthquake;

L represents the length of the surface rupture in kilometers;

D represents the displacement in meters.

In Equation 1, the length of the surface rupture and the maximum vertical displacement are confirmed via trench analysis. Thus, the magnitude of the latest event that occurred along the Tangyuan graben of the YYFZ can be estimated as ~M 7.0 based on Equation 1.

In addition, another commonly used method is the association between the severity of shaking, as measured by the modified Mercalli intensity (MMI) scale, and the lower limiting value for liquefaction effects and soft-sediment deformation, such as pseudonodules and recumbent folds (McCalpin, 2009; pubs.usgs.gov). In terms of the MMI (Wood and Neumann, 1931), soft-sediment deformation features such as folds, pseudonodules, contorted laminations, and recumbent folds often occur at MMI

values of VII (Keefer, 1984; 1999; 2002; pubs.usgs.gov), where highly susceptible sediments such as silty sand and fine sand are present. Furthermore, if liquefaction-induced ground failure occurs at the surface, the MMI may reach values of VIII–IX. Among our field observations in the trenches, coseismic deformation features such as liquid folds, contorted laminations, and recumbent folds suggest that the MMI value of the latest movement along the YYFZ in the Tangyuan graben was at least V and VI, while faulting and earthquake-induced liquefaction and associated deformation evidence such as aligned gravels along the main fault plane, sediment ejection, filling wedges, and lateral spreads imply that the MMI value of the last near-fault earthquake should not have been less than VIII and IX. In turn, we suggest that the size of the most recent paleoearthquake should not have been less than ~M 7.0 based on the empirical relationship between the MMI values investigated at the earthquake spot and the historical earthquakes (of known magnitudes).

In summary, both the magnitude estimated from the length of the surface rupture and the maximum vertical displacement directly measured in the field and the size inferred from the MMI value of the last near-fault earthquake deduced from deformation evidence such as faulting and earthquake-induced liquefaction suggest that the magnitude of the latest event occurring along the Tangyuan section of the YYFZ in the late Quaternary can be estimated as ~ M 7.0, which indicates that the fault should be viewed as a strong seismogenic structure (M≥7).

5.3 Kinematics and fault behavior of the YYFZ in the late Quaternary

Earlier studies have been carried out on the kinematic properties of the YYFZ (Min et al., 2013; Yu, 2016; Yu et al., 2016; Zhai et al., 2016; Gu et al., 2017; Shu et al., 2020), but there have been few studies on its slip rate since the late Quaternary. Although the minimum long-term slip rate of the structure was estimated to be ~0.2–0.3 mm/a based on the offset of the small gully, it was still doubted that these data may have been too few and with great uncertainty as the authors noted in their paper (Shu et al., 2020). Three uncertainties need to be reconsidered. First, modern mechanized farming in NE China would have severely disrupted and reduced the height of surface scarps and the horizontal offsets in the Late Holocene, leading to large uncertainties in the estimation of slip rate results. For example, many field investigations have found no or only relatively few scarp ridges on the surface, but the stratum dislocation revealed by the excavated trench profile is greater than the height of the surface scarp ridges (Yu et al., 2018). This special phenomenon indicates that human cultivation and industrialization in NE China has had a strong influence on the height of surface scarps, and the influence of external forces on displacements should be deeply considered in actual slip rate estimations. Moreover, the estimated long-term slip rate of ~0.2–0.3 mm/a was mainly acquired by the assumption that a coseismic displacement of ~2.8 m and a recurrence interval of ~10–20 ka are the characteristic coseismic displacement and recurrence intervals for earthquakes in the YYFZ (Shu et al., 2020). However, more studies are needed to verify whether the tectonic deformation of the YYFZ since the late Quaternary conforms to the characteristic slip model.

The faults in SCRs exhibit different spatial and temporal patterns and tectonic deformation characteristics than those at plate boundaries (Calais, et al., 2016). Our studies in the past 10 years did not reveal the features of characteristic slip in other sections, such as the Shangzhi segment and Shulan segment, along the YYFZ. Instead, the fault slip behavior is more similar to a cluster slip, with long periods of relative calmness and multiple slips occurring over short periods of time (Yu et al., 2018). In this case, there may be some uncertainty in the slip rate obtained using the characteristic recurrence interval and the characteristic displacement. Last but not least, the estimated rate of 0.2–0.3 mm/a is far below the noise level of GPS observations, which makes it unrealistic to apply these low rates of ground motion and sparse data effectively (Chen., 2021).

In this study, the right-slip rate of the Tangyuan segment of the YYFZ since the late Quaternary is constrained to 1–2 mm/a according to the upper terrace model, and we suggest that this slip rate value represents the maximum estimate. First, the Songhua River, as one of the largest rivers in NE China, exhibits ~2.1 km dextral deflection (Shu et al., 2020), and relevant research shows that the oldest river terrace of the Songhua River was formed at ~1 Ma (Yu, 2015). In this case, the average right-lateral strike-slip rate along the YYFZ can be estimated to be ~2 mm/a. This estimate is very close to the previously estimated value of ~2.3 mm/a along the TLFZ (National Seismological Bureau Institute, 1987). Based on the selected historical earthquake data and the seismic moment obtained by an empirical formula, the average slip rate of the TLFZ is calculated to be 2.65 mm/a, which is consistent with GPS observation data (Wang et al., 2009; Zheng et al., 2017; Zhang et al., 2018; Wang and Shen, 2020). The right-lateral strike-slip rates of different sections along the TLFZ have been studied using various methods, and the results are mostly concentrated at ~1–2 mm/a (Huang et al., 1993; Song et al., 2005; Jiao et al., 2016). These estimates are in good agreement with our estimate of ~1–2 mm/a.

It is also worth noting that these results are relatively concentrated, although the study sites are distributed in different sections along the TLFZ, and the study methods are different. This phenomenon seems to reveal that the strike-slip rate of the TLFZ has been consistent along the strike since the late Quaternary. However, this topic needs to be further studied in future work. Finally, the minimum long-term slip rate of the structure is estimated to be ~0.2–0.3 mm/a based on the offset of the small gully on the Tonghe segment of the YYFZ (Shu et al., 2020). We also conducted a field investigation of the Tonghe section of the YYFZ and believe that the strike-slip rate obtained by the displacement and abandonment age constraints of this gully can represent the minimum value of the YYFZ. Thus, it is suggested that the right-slip rate of the YYFZ ranges between ~0.2–0.3 mm/a (the minimum) and 1–2 mm/a (the maximum). This estimation of the slip rate is also in accordance with the recurrence interval of ~10–20 ka between strong earthquakes, which was suggested by previous studies (Min et al., 2013; Yu, 2016; Gu et al., 2017; Shu et al., 2020). This estimation of the slip rate is similar to that found in most counterparts of SCRs worldwide (Calais, et al., 2016).

Additionally, the geodynamic environment in NE China also supports the above inference. The Pacific Plate subducts westward along the Kuril Island–Japan arc-Mariana Islands line under the Eurasian Plate, and the rate of westward subduction has

slowed dramatically from approximately 13 cm/a at 80 Ma to only approximately 4 cm/a at approximately 50 Ma (Northrup et al., 1995) and at the lowest stage at ~50–30 Ma, and it has subsequently decreased further or stopped. However, over the past 10 million years, movement along the subduction zone of the Western Pacific Plate has begun to accelerate (Zhang et al., 2014). Additionally, the subduction direction of the western Pacific Plate beneath the Eurasian Plate has gradually adjusted from nearly S-N in the early Cenozoic to nearly E-W in the present (Ren et al., 2002; Yu et al., 2015b; Liu et al., 2021; 2023). In this case, the NE-trending faults on the NE China Plain, such as the YYFZ and the DMFZ, are mainly characterized by right-lateral strike-slip kinematics.

5.4 Implications for the earthquake hazard assessment and mitigation in SCRs

The study of active tectonics and seismogenic structures is useful for earthquake hazard prevention and risk mitigation, and seismic fortification standards can always be reformulated based on newly acquired quantitative data from active seismogenic faults. An increasing number of earthquakes have supported this view. For example, we were not aware of the great danger of the Longmenshan Fault Zone because of its low slip rate, and the maximum historical Ms 6.5 earthquake record until the Ms 8.0 earthquake struck Wenchuan County in 2008 (Zhang, 2013). In 2011, the Mw 9.0 Miyagi Fukushima earthquake in Japan directly resulted in a giant tsunami with a magnitude greater than the greatest magnitude recorded during the past 2,000 years, which far exceeded the seismic fortification design standards of the Fukushima nuclear power plants that were constructed before the great earthquake (Min et al., 2013). These unexpected earthquakes have caused enormous casualties and economic losses. However, the total seismic losses largely decreased in recent earthquake cases in China, such as the 2013 M 7.0 Lushan earthquake in Sichuan Province, the 2014 M 6.5 Ludian earthquake in Yunnan Province, and the 2017 M 7.0 Jiuzhaigou earthquake in Sichuan Province. Investigations after earthquakes show that the key reason for this decrease is that the quake-proof standard in these regions has been scientifically improved after the reassessment of the potential earthquake risk associated with major seismotectonic activities. These important lessons learned from previous earthquakes should be considered in the future.

The YYFZ is one of the largest structures in NE China, where the highly populated (~0.13 billion) area of China has several large heavy industry bases, agricultural centers, and academic and governmental scientific groups living directly upon it. For the Tangyuan graben of the YYFZ, there are more than 1,000,000 people living there, and the value of the maximum earthquake resistance intensity is stipulated as VI based on previous consideration. Although history records no major earthquakes (M>5) along the Tangyuan section of the YYFZ, our research clearly shows that this segment experienced at least one strong paleoearthquake in the Late Holocene with an estimated magnitude of M 7.0, which indicates that the Tangyuan segment of the YYFZ has a potential risk for large earthquakes (M≥7). This new discovery suggests that the seismic fortification standard in the Tangyuan graben urgently needs to be reformulated accordingly.

The second interesting feature that needs to be considered is the spatial migration of the fault slip. This research revealed that a new active fault trace is situated within the Tangyuan graben interior (Figures 4–10), which implies that the latest activity migrated into the graben interior from the previous boundary faults. Similar features have also been revealed on other segments of the TLFZ (Mi et al., 2013; Min et al., 2013; Yu et al., 2018; Shu et al., 2020). The migration or transition of fault activity from boundary faults to new faults in the basin interior may represent an important evolutionary step in the formation and development of the structure, which means that the short new active segments in the basin interior along different sections may be integrated into a long segment in the future, ultimately forming a new structure. Thus, the presence of new faults in the basin interior, in addition to boundary faults, merits special attention when assessing the influential surface range and strong earthquake potential.

Furthermore, the "migration in space and clustered in time" activity observed along the YYFZ has also been observed in many other SCRs, such as the North China Plain, Western Europe, central and eastern U.S., and Duren, Germany (Calais et al., 2016), where only sparse or sporadic strong earthquakes and long intervals of seismic quiescence have been documented, the strain accumulation rate has been too low to be recognized, and single or episodic activity has been revealed by most SCR faults (Calais et al., 2016). Under these circumstances, earthquake events in time and space in SCRs are more likely triggered by transient perturbations of stress or fault strength than by the slow accumulation of tectonic stress on long-lived active faults (Calais et al., 2016), which completely differ in spatial and temporal patterns from their counterparts at plate boundaries, such as the San Andreas fault on the west coast of the United States.

The YYFZ is located in NE China, where few strong earthquake events have been recorded, the current strain accumulation rate is very low, and the strong earthquake recurrence period is as long as 10–20 ka, as shown by paleoseismic data (Mi et al., 2013; Min et al., 2013; Yu et al., 2018; Shu et al., 2020), which are similar to those of the remaining segments of the TLFZ (Yang et al., 2006; Cao et al., 2015; Yang et al., 2017; Shu et al., 2020). All of these features are also very similar to the tectonic deformation observed in other faults in other SCRs of the world (Calais et al., 2016). In other words, NE China may be regarded as a typical SCR. If that is the case, the seismic hazard in the YYFZ, even the whole TLFZ, cannot be determined only by the low tectonic loading rate and sporadic and clustered seismicity, and more future research needs to be carried out to reconsider its earthquake occurrence mechanisms and the hazard mitigation measures in NE China.

Markedly different from other SCRs, the special composition of regional basement material, recent volcanic activity, and modern artificial modification are three important factors that need to be considered in the study of active tectonics and seismic geology in NE China. First, the mechanical properties of the basement in NE China should be given more consideration. The earthquake activity recorded along the TLFZ is influenced not only by the fault but also by the mechanical properties of the basement material. The North China Craton, composed of rigid basement rocks from the Archean era, often experiences stress concentrations along basement faults, leading to frequent large earthquakes (such as the 70 BC M 7 Anqiu earthquake, 1668 M 8½ Tancheng earthquake, 1976 M 8 Tangshan

earthquake, and several M 7–7.5 earthquakes from 1548 to 1975 offshore in Bohai Bay; Shu et al., 2020). In contrast, the South China Block is composed of flexible basement rocks that are early to middle Proterozoic in age, where stress is often released through basement deformation, resulting in fewer earthquakes (Liu et al., 2021; 2023). The basement of NE China shares similarities with that of the South China Block, primarily consisting of flexible basement rocks. A recent study revealed that NE China consists of two Precambrian blocks and three accretionary terranes. These include the Xing'an accretionary terrane (XAT), Songliao accretionary terrane (SAT), and Zhangguangcai accretionary terrane (ZGCAT), which are separated from each other by the Xinlin-Xiguitu suture (XXS), Hegenshan-Heihe suture (HHS), Longfengshan suture (LFS), and Mudanjiang-Yilan suture (MYS), respectively. The YYFZ is located at the boundary between the SAT and the ZGCAT and is considered a complex mosaic terrane association without an integrated and rigid basement (Liu et al., 2021, 2022). Considering such characteristics of basement material composition, the frequency and intensity of earthquakes in NE China may be weaker than those in the North China Craton area. Second, influenced by the oblique subduction of the Pacific Plate, more deep-source earthquakes (with focal depths ≥300 km) and more intense Cenozoic volcanic activity have occurred in NE China (Huang et al., 2006). These tectonic activities may greatly release the accumulated energy. As a result, strong seismic events that can propagate to the surface and form significant coseismic surface ruptures may be relatively rare. Strong volcanic eruptions and deep earthquakes along the Dunhua–Mishan Fault Zone are typical examples (Figure 1). If this is the case, it is assumed that the intensity of tectonic movement in NE China is not weak, but the method of energy release is quite different from that in other regions. Finally, NE China has a flat terrain; is influenced by significant erosion from rainfall, ice, and snow; and is a modern farming center of the country. Large-scale mechanized farming and modern human activities may destroy the surface coseismic deformation characteristics once they develop near the fault zone. In other words, the surface deformed features are destroyed and difficult to preserve. If this is the case, more detailed field investigation work will need to be analyzed and verified by historical remote-sensing images. In summary, the above three factors are important to consider, especially when we analyze and evaluate the risk of strong earthquakes in NE China.

6 Conclusion

Based on the integrated data on high-precision satellite image interpretation, detailed geological and geomorphological investigations, seismic reflections, and Quaternary chronological testing, the following results can be presented:

(1) A linear belt of geomorphologic anomalies more than 15 km long was revealed in the Tangyuan graben interior of the YYFZ, the northern segment of the TLFZ, and a series of sag ponds, scarps, and small bulges elongated parallel to the surface geomorphic belt were described.
(2) Trenches and seismic reflections revealed that the belt corresponds to a newly developed fault in the graben interior and that the latest tectonic deformation of the YYFZ migrated into the new fault in the graben interior from the previous boundary faults, and at least one paleoearthquake with an estimated magnitude of M 7.0 can be verified in the trenches. The dating of the samples confirmed that this latest rupturing event might have occurred between 2,800± 600 a BP and 1,700 ± 200 a BP, which resulted in 0.8 ± 0.1 m of maximum vertical coseismic displacement with normal strike-slip kinematics.
(3) The measured maximum cumulative right-lateral offset of the T2 terrace of the Heijin River in the Tangyuan graben may reach 110 ± 5 m with an abandonment age of ~55.13 ± 1.78 ka (OSL), which suggests that the maximum right-slip rate of the YYFZ since the late Quaternary is ~1–2 mm/a based on the upper terrace model.
(4) The Tangyuan segment of the YYFZ is a seismogenic structure for strong earthquakes (M≥7), and new seismic hazard and fortification standards are urgently needed. The features of "low tectonic loading rate, activity migration in space, and clustering in time separated by 10,000 years of seismic quiescence" observed along the YYFZ in NE China are highly important for earthquake model construction and tectonic deformation studies in stable continental regions.

Data availability statement

The raw data supporting the conclusion of this article will be made available by the authors, without undue reservation.

Author contributions

ZY: conceptualization, funding acquisition, investigation, and writing–review and editing. NY: methodology, project administration, and writing–original draft. YY: data curation, investigation, and writing–review and editing. LL: investigation, validation, visualization, and Writing–review and editing. YM: formal analysis, software, and writing–review and editing.

Funding

The author(s) declare that financial support was received for the research, authorship, and/or publication of this article. This work was jointly supported by the Central University Basic Research Funds of College of Disaster Prevention (Grant No. 20215110), China Postdoctoral Science Foundation (Grant No. 2018M631534), and the Special Fund of the Institute of Geophysics, China Earthquake Administration (Grant No. DQJB18B21).

Acknowledgments

The authors would like to sincerely acknowledge the assistance of Pei-zhen Zhang, Wei Min, Wen-jun Zhen, Qing-Hai Wei, Hua Pan, Jin-chen Li, Yu-gang Liu, Shuang Liu, Jian Kang, Xin-lan Li, Hai-feng Sun, Li-cheng Zhang, and Bin Zhao for their help both in the laboratory and in the field. The authors also sincerely

acknowledge the editors and reviewers for their constructive comments and suggestions.

Conflict of interest

The authors declare that the research was conducted in the absence of any commercial or financial relationships that could be construed as a potential conflict of interest.

Publisher's note

All claims expressed in this article are solely those of the authors and do not necessarily represent those of their affiliated organizations, or those of the publisher, the editors, and the reviewers. Any product that may be evaluated in this article, or claim that may be made by its manufacturer, is not guaranteed or endorsed by the publisher.

References

Audemard, F., Pantosti, D., Machette, M., Costa, C., Okumura, K., Cowan, H., et al. (1999). Trench investigation along the Mérida section of the Boconó fault (central Venezuelan Andes), Venezuela. *Tectonophysics* 308, 1–21. doi:10.1016/s0040-1951(99)00085-2

Calais, E., Camel beeck, T., Stein, S., Liu, M., and Craig, T. J. (2016). A new paradigm for large earthquakes in stable continental plate interiors. *Geophys. Res. Lett.* 43 (20), 10,621–10,637. doi:10.1002/2016GL070815

Cao, J., Ran, Y., Xu, H., Zhang, P., Ma, X., and Li, L. (2015). Typical case analysis on application of multi-method detection technique to active fault exploration in Suqian city. *Seismol. Geol.* 35, 430–439.

Cetin, H., Guneyli, H., and Mayer, L. (2003). Paleoseismology of the palu-lake hazar segment of the east anatolian Fault Zone, Turkey. *Tectonophysics* 374, 163–197. doi:10.1016/j.tecto.2003.08.003

Chen, W. P. (2021). Spatial patterns of seismogenic faulting in northeastern Asia. *Earth-Science Rev.* 220, 103704–112048. doi:10.1016/j.earscirev.2021.103704

Deng, Q. D., Ran, Y. K., Yang, X. P., Min, W., and Chu, Q. Z. (2007). *Active tectonics map of China (1:4 million)*. Beijing, China: Seismological Press, 2–3. (in Chinese with English abstract).

Deng, Q. D., Yu, G. H., and Ye, W. H. (1992). "Study on the relations between parameters of surface rupture and magnitude," in *Research on active fault (2)*. Editor SSB (Beijing, China: Institute of Geology, Seismological Press), 247–264. (in Chinese with English abstract).

Geology and Mineral Resources Bureau of Heilongjiang Province (1993). *Regional geology of Heilongjiang Province*. Beijing, China: Geologic Publishing House, 115–145. (in Chinese with English abstract).

Gu, C. C., Zhu, G., Zhai, M. J., Lin, S. Z., Song, L. S., and Liu, B. (2016). Features and origin time of mesozoic strike-slip structures in the Yilan-Yitong Fault Zone. *Sci. Chin. Earth Sci.* 59, 2389–2410. doi:10.1007/s11430-016-5334-4

Gu, C. C., Zhu, G., Zhang, S., Liu, C., Li, Y., Shao, L. S., et al. (2017). Cenozoic evolution of the Yilan-Yitong graben in NE China: an example of graben formation controlled by pre-existing structures. *J. Asian Earth Sci.* 146, 168–184. doi:10.1016/j.jseaes.2017.05.024

Houtgast, R. F., Van Balen, R. T., and Kasse, C. (2005). Late quaternary evolution of the feldbiss fault (roer valley rift system, The Netherlands) based on trenching, and its potential relation to glacial unloading. *Quat. Sci. Rev.* 24, 491–510.

Hsiao, L., Graham, S. A., and Tilander, N. (2004). Seismic reflection imaging of a major strike-slip fault zone in a rift system: Paleogene structure and evolution of the Tan-Lu fault system, Liaodong Bay, Bohai, offshore China. *AAPG Bull.* 88 (1), 71–97. doi:10.1306/09090302019

Huang, J. L., and Zhao, D. P. (2006). High-resolution mantle tomography of China and surrounding regions. *Solid earth.* 111 (B9), B09305. doi:10.1029/2005JB004066

Huang, W. (1993). Morphologic patterns of stream channels on the active Yishi Fault, southern Shandong Province, Eastern China: implications for repeated great earthquakes in the Holocene. *Tectonophysics* 219, 283–304. doi:10.1016/0040-1951(93)90179-n

Huggett, R. J. (2011). *Fundamentals of geomorphology*. 3rd edition. London, UK: Routledge, 86.Size grades of sedimentary particles

Jiao, Q., Jiang, W., Zhang, J., Jiang, H., Luo, Y., and Wang, X. (2016). Identification of paleoearthquakes based on geomorphological evidence and their tectonic implications for the southern part of the active Anqiu-Juxian fault, eastern China. *J. Asian Earth Sci.* 132, 1–8. doi:10.1016/j.jseaes.2016.10.012

Keefer, D. K. (1984). Landslides caused by earthquakes. *Geol. Soc. Am. Bull.* 95, 406–421. doi:10.1130/0016-7606(1984)95<406:lcbe>2.0.co;2

Keefer, D. K. (1999). Earthquake-induced landslides and their effects on alluvial fans. *J. Sed. Res.* 69, 84–104. doi:10.1306/d4268978-2b26-11d7-8648000102c1865d

Keefer, D. K. (2002). Investigating landslides caused by earthquakes—a historical review. *Surv. Geophys.* 23, 473–510. doi:10.1023/a:1021274710840

Lafuente, P., Arlegui, L. E., Liesa, C. L., and Simon, J. L. (2011). Paleoseismological analysis of an intraplate extensional structure the Concud fault (Iberian Chain, eastern Spain). *Int. J. Earth Sci. Geol. Rundsch* 100, 1713–1732. doi:10.1007/s00531-010-0542-1

Li, H. B., Van derwoerd, J., Sun, Z. M., Meriaux, S. A., Tapponnier, P., Ryerson, J. F., et al. (2008). Late quaternary left-slip rate and large earthquake recurrence time along the kangxiwar (or karakax) segment of the altyn tagh fault, northern tibet. *Quat. Sci.* 28 (2), 198–213.

Li, X. F., Chen, Q. M., Zhang, X. H., Zhang, C. H., Zhang, F. S., and Zhang, Z. W. (2002). The Yitong Graben-the structural features and evolution of a strike-slip fault basin. *Petrol. Geol. Exp.* 24 (1), 19–24. (in Chinese with English abstract).

Li, Z. G., Jiao, D., Chen, W., Zhang, Y. K., Wang, M. M., Li, Y., et al. (2013). Structural deformation and evolution of right-lateral strike-slip tectonics of the Liaohe western depression during the early Cenozoic. *J. Asian Earth Sci.* 77, 1–11. doi:10.1016/j.jseaes.2013.08.002

Liu, J. R., Ren, Z. K., Min, W., Ha, G. H., and Lei, J. B. (2021). The advance in obtaining fault slip rate of strike slip fault-A review. *Earthq. Res. Adv.* 1, 100032. doi:10.1016/j.eqrea.2021.100032

Liu, M. Q., Yang, B. Z., Deng, J. G., and Zhou, Y. H. (1993). *Geological tectonic features and evolution of yitong-shulan graben*. Beijing, China: Geological Publishing House, 1–106. (in Chinese with English abstract).

Liu, Y. J., Li, W. M., Ma, Y. F., Feng, Z. Q., Guan, Q. B., Li, S. Z., et al. (2021). An orocline in the eastern central asian orogenic belt. *Earth-Science Rev.* 221, 103808–103833. doi:10.1016/j.earscirev.2021.103808

Liu, Y. J., Xiao, W. J., Ma, Y. F., Li, S. Z., Peskov, A. Y., Chen, Z. X., et al. (2023). Oroclines in the central asian orogenic belt. *Natl. Sci. Rev.* 10 (2), nwac243–3. doi:10.1093/nsr/nwac243

Liu-Zeng, J., Wang, P., Zhang, Z., Li, Z., Cao, Z., Zhang, J., et al. 2017. Liquefaction in western sichuan basin during the 2008 Mw 7.9 wenchuan earthquake, China. *Tectonophysics*, 694, 214–238, doi:10.1016/j.tecto.2016.11.001

Lu, Y. C., Wang, X. L., and Wintle, A. G. (2007). A new OSL chronology for dust accumulation in the last 130,000 yr for the Chinese Loess Plateau. *Quat. Res.* 67 (1), 152–160. doi:10.1016/j.yqres.2006.08.003

McCalpin, J. P. (1996). *Paleoseismology*. California, UK: Academic Press.

McCalpin, J. P. (2009). *Paleoseismology*. California, UK: Academic Press.

Mi, X. N., Liu, Y. J., Jiang, T., Liang, C. Y., Tang, Z. X., and Li, W. M…Cui, F.S. (2013). Structural characteristics and evolution of the shulan basin. *Geol. Bull. Chin.*, 32 (4), 589–600 (in Chinese with English abstract).

Min, W., Jiao, D. C., Zhou, B. G., Sheng, J., and Chen, T. (2011). The significance of discovery on Holocene activity on the Yilan-Yitong fault in northeast China. *Seismol. Geol.* 01, 74–79. (in Chinese with English abstract).

Min, W., Liu, Y. G., Jiao, D. C., Shen, J., and Pan, X. D. (2013). Evidence for Holocene activity of the Yilan-Yitong fault, northeastern section of the Tan-Lu fault zone in Northeast China. *J. Asian Earth Sci.* 67–68, 207–216. doi:10.1016/j.jseaes.2013.02.031

Philip, G., Bhakuni, S. S., and Suresh, N. (2012). Late Pleistocene and Holocene large magnitude earthquakes along himalayan frontal thrust in the central seismic gap in NW himalaya, kala amb, India. *Tectonophysics* 580, 162–177. doi:10.1016/j.tecto.2012.09.012

Ren, J. Y., Lu, Y. C., Li, S. T., Yang, S. G., and Zhuang, X. G. (1999). The tectonic evolution of Yishu Graben and its depositional filling response. *Chin. Geol. Sin.* 34 (2), 196–203. (in Chinese with English abstract).

Ren, J. Y., Tamaki, K., Li, S. T., and Zhang, J. X. (2002). Late Mesozoic and Cenozoic rifting and its dynamic setting in Eastern China and adjacent areas. *Tectonophysics* 344 (3), 175–205. doi:10.1016/s0040-1951(01)00271-2

Ren, Z., Zhang, Z., Chen, T., and Wang, W. (2013). Theoretical and quantitative analyses of the fault slip rate uncertainties from single event and erosion of the accumulated offset. *Isl. Arc* 22 (2), 185–196. doi:10.1111/iar.12015

Shen, Y., Liu, C., Jiang, L., Wang, S. Y., and Wang, D. (2006). Fault characteristics and analysis of tectonic styles in Tangyuan Fault-depression. *J. Jilin Univ. (Earth Sci. Ed.)* 36 (11), 104–108. (in Chinese with English abstract).

Shu, P., Min, W., Liu, Y. G., Xu, X. W., Li, K., Yu, Z. Y., et al. (2020). Late Quaternary paleoseismology and faulting behavior of the Yilan-Yitong fault zone and implications for seismic hazards of the Tanlu fault zone, eastern China. *J. Asian Earth Sci.* 201, 104509–104517. doi:10.1016/j.jseaes.2020.104509

Song, F. M., Yang, X. P., He, H. L., et al. (2005). Quantitative analysis of recent activity of the xiaodianzi-maobu segment of the anqiu-juxian fault, Shandong Province (in Chinese). *Seismol. Geol.* 27, 200–211.

Sun, X. M., Long, S. X., Zhang, M. S., Liu, X. Y., and Hao, F. J. (2006). Discovery and timing of major thrust belt in Jiamusi-Yitong fault zone. *Oil Gas. Geol.* 27, 637–643. (in Chinese with English abstract).

Sylvester, A. G. (1988). Strike-slip faults. *Geol. Soc. Am. Bull.* 100 (100), 1666–1703. doi:10.1130/0016-7606(1988)100<1666:ssf>2.3.co;2

Tang, D. Q., Chen, H. H., Sun, J. Z., Zhang, H., and Chen, L. (2010). Cenozoic tectonic evolution of the Yitong part of the Tan-Lu fault zone and its control on Yitong Basin. *Geotect. Metall.* 34 (3), 340–348. (in Chinese with English abstract).

Tang, D. Q., He, S., Chen, H. H., Jiang, T., and Qiu, Y. C. (2009). Fault system's characteristics of Yitong Basin and its evolution. *J. Jilin Univ. (Earth Sci. Ed.)* 39 (3), 386–396. (in Chinese with English abstract).

Tian, Z. Y., and Du, Y. L. (1987). Formation and evolution of the yilan–yitong graben. *Tectonophysics* 133 (3), 165–173. doi:10.1016/0040-1951(87)90261-7

Tocher, D. (1958). Earthquake energy and ground breakage. *BSSA* 48, 147–153. doi:10.1785/bssa0480020147

Tong, H. M. (2002). The property and evolution of boundary faults of Yitong Graben. *J. Geomech.* 8 (1), 35–42. (in Chinese with English abstract).

Vanneste, K., Meghraoui, M., and Camelbeeck, T. (1999). Late quaternary earthquake-related soft-sediment deformation along the Belgian portion of the feldbiss fault, lower rhine graben system. *Tectonophysics* 309, 57–79. doi:10.1016/s0040-1951(99)00132-8

Wang, W. T. (2007). *Sedimentary response of Tangyuan fault basin to the uplifting history of provenances in the Paleogene*. Changchun, China: Jilin University, 6–87. (in Chinese with English abstract).

Wells, D. L., and Coppersmith, K. J. (1994). New empirical relationships among magnitude, rupture length, rupture width, rupture area, and surface displacement. *Bull. Seismol. Soc. Am.* 84 (4), 974–1002. doi:10.1785/bssa0840040974

Wesnousky, S. G. (2006). Predicting the endpoints of earthquake ruptures. *Nature* 444 (7117), 358–360. doi:10.1038/nature05275

Wood, H. O., and Neumann, F. (1931). Modified Mercalli intensity scale of 1931. *Bull. Seis. Soc. Am.* 21, 277–283. doi:10.1785/bssa0210040277

Xu, J. W., and Zhu, G. (1994). Tectonic models of the Tan–Lu fault zone, eastern China. *Int. Geol. Rev.* 36 (8), 771–784. (in Chinese). doi:10.1080/00206819409465487

Xu, J. Y. (1997). Tectonic evolution of yishu graben in cenozoic. *Earth Sci.–J. Chin. Univ.Geosci.* 22 (4), 406–410. (in Chinese with English abstract).

Xu, M., Li, Y. L., Hou, H. S., Wang, C. S., Gao, R., Wang, H. Y., et al. (2017). Structural characteristics of the yilan–yitong and dunhua–mishan faults as northern extensions of the tancheng–lujiang Fault Zone: new deep seismic reflection results. *Tectonophysics* 706-707, 35–45. doi:10.1016/j.tecto.2017.03.018

Yang, C. Z., Ren, J. Y., Zhang, Z. Y., and Zhang, J. X. (2014). Cenozoic structural characteristics and evolution in the Fangzheng fault depression. Northeast China. *Geotect. Metall.* 38 (2), 388–397. (in Chinese with English abstract).

Yang, J. G., Liu, J. L., Wu, H. Y., and Liu, C. G. (2007). The characteristics and evolvement of the tectonic in Tangyuan rift in northern Heilongjiang. *J. Daqing Petrol. Inst.* 31 (1), 19–21. (in Chinese with English abstract).

Yang, X., Song, F., Zhang, L., He, H., Li, C., and Wang, Z. (2006). A recent paleoearthquake on Qingfengling seismic fault of Tanlu fault zone. *Acta Seismol. Sin.* 19, 225–230. doi:10.1007/s11589-002-0225-5

Yang, Y. Y., Zhao, H. G., Yao, D. D., Wang, X. Z., Miao, P., Li, J. H., et al. (2017). Evidence of Holocene activity discovered in Anhui Ziyangshan segment of Tanlu fault zone. *Seismol. Geol.* 39, 644–655.

Yeats, R. S., Sieh, K., and Allen, C. R. (1997). *The geology of earthquakes*. Oxford, UK: Oxford University Press, 44–67.

Yin, A. (2010). Cenozoic tectonic evolution of Asia: a preliminary synthesis. *Tectonophysics* 488, 293–325. doi:10.1016/j.tecto.2009.06.002

Yin, A., and Nie, S. Y. (1993). An indentation model for the North and South China collision and the development of the Tan-Lu and Honam fault systems, eastern Asia. *Tectonics* 12 (4), 801–813. doi:10.1029/93tc00313

Yu, Z. Y. (2016). Late Quaternary tectonic deformation and active behavior of segmentation of the Yilan-Yitong fault zone, NE China. *Inst. Seismol. Geol. China Earthq. Adm.*, 39–298. (in Chinese with English abstract).

Yu, Z. Y., Min, W., Wei, Q. H., Zhao, B., and Ma, Y. C. (2015a). The geometric characteristics and tectonic deformation mechanism of inversion structures in northern songliao Basin and their seismo–geological significance: a case from Da'an–Dedu fault. *Seismol. Geol.* 37 (1), 13–32. (in Chinese with English abstract).

Yu, Z. Y., Yin, N., Shu, P., Li, J. C., Wei, Q. H., Min, W., et al. (2018). Late quaternary paleoseismicity and seismic potential of the Yilan-Yitong Fault Zone in NE China. *J. Asian Earth Sci.* 151, 197–225. doi:10.1016/j.jseaes.2017.10.038

Yu, Z. Y., Zhang, P. Z., Min, W., Wei, Q. H., Liu, Y. G., and Liu, S. (2016). Late Holocene average recurrence interval of great earthquakes of Shangzhi part of the Yilan-Yitong Fault Zone, NE China: constraints from paleo-earthquakes and historical written records. *Seismol. Geol.* 38 (4), 843–861. (in Chinese with English abstract).

Yu, Z. Y., Zhang, P. Z., Min, W., Wei, Q. H., Wang, L. M., Bin, Z., et al. (2015b). Late cenozoic deformation of the da'an-dedu Fault Zone and its implications for the earthquake activities in the songliao basin, NE China. *J. Asian Earth Sci.* 107, 83–95. doi:10.1016/j.jseaes.2015.03.047

Zhai, M. J., Zhu, G., Liu, B., Gu, C. C., Zhang, S., Lin, S. Z., et al. (2016). Analysis on neotectonic activity of the yilan -Yitong fault. *Chin. J. Geol.* 51 (2), 594–618. (in Chinese with English abstract).

Zhang, P. Z. (2013). Beware of slowly slipping faults. *Nat. Geosci.* 6 (5), 323–324. doi:10.1038/ngeo1811

Zhang, P. Z., Deng, Q. D., Zhang, G. M., Ma, J., Gan, W. J., Min, W., et al. (2003). Active tectonic blocks and strong earthquakes in the continent of China. *Sci. China Ser. D Earth Sci.* 46, 13–24. doi:10.1360/03dz0002

Zhang, P. Z., Li, C. Y., and Mao, F. Y. (2008). Strath terrace formation and strike-slip faulting. *Seismol. Geol.* 30 (1), 44–57.

Zhang, P. Z., Molnar, P., and Xu, X. (2007). Late quaternary and present-day rates of slip along the altyn tagh fault, northern margin of the Tibetan plateau. *Tectonics* 26, 1–24. doi:10.1029/2006tc002014

Zhang, P. Z., Zhang, H. P., Zheng, W. J., Zheng, D. W., Wang, W. T., and Zhang, Z. Q. (2014). Cenozoic tectonic evolution of continental eastern Asia. *Seismol. Geol.* 36 (3), 574–585.

Zhang, P. Z., Zheng, W. J., Zheng, D. W., Wang, W. T., and Zhang, Z. Q. (2014). Cenozoic tectonic evolution of continental Eastern Asia. *Seismol. Geol.* 36 (3), 574–585. (in Chinese with English abstract).

Zhang, Q. L., Wang, L. S., Xie, G. A., Du, J. M., Xu, S. Y., and Hu, X. Z. (2005). Discussion on northward extension of Tanlu fault zone and its tectonic regime transformation. *Geol. J. China Univ.* 11 (4), 577–584. (in Chinese).

Zhang, Y., and Wang, X. K. (1995). *Research on neotectonic movement in the manzhouli–suifenhe geoscience transection*. Changchun, China: Jilin University Press, 73–74. (in Chinese with English abstract).

Zhang, Y. G., Zheng, W. J., Wang, Y. J., Zhang, D. L., Tiyan, Y. T., Wang, M., et al. (2018). Contemporary deformation of the North China plain from global positioning system data. *Geophys. Res. Lett.* 45, 1851–1859. doi:10.1002/2017gl076599

Zhao, T., Zhu, G., Lin, S. Z., and Wang, H. Q. (2016). Indentation-induced tearing of a subducting continent: evidence from the tan–Lu Fault Zone, east China. *Earth-Sci. Rev.* 152, 14–36. doi:10.1016/j.earscirev.2015.11.003

Zheng, L. S., Gao, W. M., and Zheng, C. B. (1988). Segmentation of the Tan-Lu fault zone and activity of the Yishu fault. *Earthq. Res. China* 4 (3), 123–129. (in Chinese with English abstract).

Zhu, G., Hu, W., Song, L. H., and Liu, B. (2015). Quaternary activity along the tan–Lu fault zone in the Bohai Bay, east China: evidence from seismic profiles. *J. Asian Earth Sci.* 114, 5–17. doi:10.1016/j.jseaes.2015.03.030

Zhu, G., Liu, G. S., Niu, M. L., Xie, C. L., Wang, Y. S., and Xiang, B. W. (2009). Syn-collisional transform faulting of the Tan-Lu fault zone, East China. *Int. J. Earth Sci.* 98 (1), 135–155. doi:10.1007/s00531-007-0225-8

Zhu, G., Wang, W., Gu, C. C., Zhang, S., and Liu, C. (2016). Late mesozoic evolution history of the tan-Lu Fault Zone and its indication to destruction processes of the North China Craton. *Acta Petrol. Sin.* 32 (4), 935–949. (in Chinese with English abstract).

Zhu, G., Wang, Y. S., Liu, G. S., Niu, M. L., Xie, C. L., and Li, C. C. (2005). $^{40}Ar/^{39}Ar$ dating of strike-slip motion on the Tan-Lu fault zone. East China. *J. Struct. Geol.* 27 (8), 1379–1398. doi:10.1016/j.jsg.2005.04.007